

In memory of my mother

To my father

(I owe them everything)

To Zehra and Moumène with gratitude

BEHAVIOR OF CCT NODES IN STRUCTURAL
CONCRETE STRUT-AND-TIE MODELS

BY

ABDELHAKIM BOUADI

THESIS

Presented to the Faculty of the Graduate School of
The University of Texas at Austin
in Partial Fulfillment
of the Requirements
for the Degree of
MASTER OF SCIENCE IN ENGINEERING

THE UNIVERSITY OF TEXAS AT AUSTIN

DECEMBER 1989

ACKNOWLEDGEMENTS

The research described herein was conducted at the Phil M. Ferguson Structural Engineering Laboratory and was made possible through funding provided by the Texas State Department of Highways and Transportation.

The author wishes to express his sincere gratitude to Dr. J.O. Jirsa for his patience and guidance throughout this work. Thanks are extended to Dr. J.E. Breen for his helpful suggestions and for serving as a second reader. Special thanks are also expressed to Dr. M.E. Kreger. Konrad Bergmeister contribution is gratefully appreciated.

The author extends his thanks to the Phil M. Ferguson Laboratory staff including Blake Stasney, Patrick Ball, Richard Marshall, Alec Tahmassebi, Wayne Little, Robert Garcia, Wayne Fontenot, Laurie Golding, Jean Gehrke, Jennifer Batson, Sharon Gunningham, Irene Moore, Maxine DeButts.

The author is indebted to all his follow graduate students for their help and friendship, specially Randy Bravo, Tony Powers, Jose Pincheira, Donna Mader, David Sanders, Larbi Sennour, and Sergio Alcocer. Thanks also to Krim Sellidj for his friendship and valuable help in putting this manuscript together.

TABLE OF CONTENTS

CHAPTER 1	INTRODUCTION	1
1.1	General	1
1.2	Background	1
1.3	Objective of the Study	6
CHAPTER 2	SPECIMEN DETAILS	9
2.1	Geometry of Test Specimens	9
2.2	Specimen Details	13
CHAPTER 3	EXPERIMENTAL INVESTIGATION	21
3.1	Materials	21
3.1.1	Concrete	21
3.1.2	Reinforcing Steel	21
3.2	Instrumentation	24
3.2.1	Strain Gages	24
3.2.2	Linear Potentiometers	24
3.2.3	Demec Gage Readings	24
3.3	Specimen Fabrication	32
3.4	Experimental Setup	34
3.5	Test Procedure	36
3.5.1	Preparation for Testing	36
3.5.2	Loading Procedure	37
3.5.3	Data Collection	39
CHAPTER 4	EXPERIMENTAL RESULTS	41
4.1	Results Presented	41
4.2	Individual Specimen Test Results	41
4.3	Comparison of Experimental Results	87
4.3.1	Failure Mode	87
4.3.2	Rebar Force	93

	4.3.3 Surface Strain	93
CHAPTER 5	EVALUATION OF TEST RESULTS	94
5.1	Introduction	94
5.2	Node Geometry	94
5.3	Specimen Failing in Compression	96
	5.3.1 Experimental Data	96
	5.3.2 Comparison to Existing Solutions	96
	5.3.2.1 Thürlimann	96
	5.3.2.2 Collins and Mitchell	99
	5.3.2.3 Nielsen et al	99
	5.3.2.4 Schlaich et al	100
	5.3.2.5 Conclusions	100
5.4	Specimen Failing in Anchorage	101
	5.4.1 Experimental Data	101
	5.4.2 Effective Anchorage Length	101
	5.4.3 Required Anchorage Length (ACI 318-83)	101
	5.4.4 Required Anchorage Length using ACI408	101
	5.4.5 Comparison	102
	5.4.5.1 Comparison to ACI 318	107
	5.4.5.2 Comparison to ACI 408	107
	5.4.6 Conclusions	108
5.5	Need for Further Research	109
CHAPTER 6	CONCLUSIONS	110
6.1	Introduction	110
6.2	Conclusions and Recommendations	110

LIST OF TABLES

Table	Page
2.1 Summary of Series I	20
2.2 Summary of Series II	20
3.1 Concrete Mix Design for Series I (A1,B1,A2, B2,A1-R)	22
3.2 Concrete Mix Design for Series II (A1-2,C1,D1,D2)	22
3.3 Concrete Strength	27
3.4 Reinforcement Properties	27
4.1 Failure Mode of Test Specimens	92
5.1 Specimen Dimensions	97
5.2 Bar Development Length	97
5.3 Compressive Stresses and Efficiency Factors	98
5.4 Experimental and Analytical Efficiency Factors	98

5.5	Specimens with Anchorage Failure: Provided and Computed Length to Develop Failure	103
5.6	Specimens with Anchorage Failure: Computed and Measured Force in Bars at Failure	103
5.7	Comparison Between Computed and Measured Force in Bars	105
5.8	Effect of Lateral Pressure	105

LIST OF FIGURES

Figure	Page
1.1 Strut and Tie Model for a Beam	3
1.2 Examples of Strut and Tie Model (From Ref. 17). .	3
1.3 Strut and Tie Model for the Prototype Dapped Beam	4
1.4 Prototype Dapped Beam Crack Pattern (From Ref.3)	5
1.5 Effect of Reinforcement Layout on CCT Node Dimensions (From Ref. 2)	8
2.1 Original Dapped Beam	10
2.2 Stress Trajectories (From Ref.2)	11
2.3 Strut Angle for the CCT Node Investigated	12
2.4 Series I Details (Specimens A1, B1, A2, B2, A1-R)	14
2.5 Reinforcement Configuration of Series I Specimens	15

2.6	Bearing Area, Series I	16
2.7	Reinforcement Configuration of Series II	18
3.1	Concrete Strength vs. Time Curve for Concrete Used in Series I (A1, A2, B1, B2, A1-R)	23
3.2	Concrete Strength vs. Time Curve for Concrete Used in Series II (A1-2, C1, D1, C2, D2)	23
3.3	Strain-Stress Curve for #3 Grade 60 Reinforcing Bar	25
3.4	Strain-Stress Curve for #53 Grade 60 Reinforcing Bar	25
3.5	Strain-Stress Curve for #6 Grade 60 Reinforcing Bar	26
3.6	Strain-Stress Curve for #7 Grade 60 Reinforcing Bar	26
3.7	Strain Gage Location	28
3.8	Linear Potentiometer Location	29
3.9	Location of Demec Points for Surface Strain Measurements	30

3.10	Steel Cage and Formwork	33
3.11	Elevation of Test Setup	35
3.12	Specimen in Place Under the Loading Machine . . .	38
4.1	Typical Specimen Load-Vertical Deflection Curve	42
4.2	Specimen A1-2 Crack Pattern	44
4.3	Specimen A1 At Failure	45
4.4	Stresses and Total Force in Longitudinal Bars (Specimen A1)	46
4.5	Specimen A1 Surface Strain (Not Principal) . . .	48
4.6	Specimen B1 Crack Pattern	49
4.7	Specimen B1 At Failure	50
4.8	Stresses and Total Force in Longitudinal Bars (Specimen B1)	51
4.9	Specimen B1 Surface Strain (Not Principal) . . .	53
4.10	Specimen A2 Crack Pattern	54
4.11	Specimen A2 At Failure	55

4.12	Stresses and Total Force in Longitudinal Bars (Specimen A2)	56
4.13	Specimen A2 Surface Strain (Not Principal) . . .	57
4.14	Specimen B2 Crack Pattern	59
4.15	Specimen B2 At Failure	60
4.16	Stresses and Total Force in Longitudinal Bars (Specimen B2)	61
4.17	Specimen B2 Principal Surface Strain	62
4.18	Specimen A1-R Crack Pattern	63
4.19	Specimen A1-R At Failure	65
4.20	Stresses and Total Force in Longitudinal Bars (Specimen A1-R)	66
4.21	Specimen A1-R Principal Surface Strain . . .	67
4.22	Specimen A1-2 Crack Pattern	68
4.23	Specimen A1-2 At Failure	69
4.24	Stresses and Total Force in Longitudinal Bars (Specimen A1-2)	71

4.25	Specimen A1-2 Principal Surface Strain	72
4.26	Specimen C1 Crack Pattern.	73
4.27	Specimen C1 At Failure	74
4.28	Stresses and Total Force in Longitudinal Bars (Specimen C1).	75
4.29	Specimen C1 Principal Surface Strain	77
4.30	Specimen C2 Crack Pattern.	78
4.31	Specimen C2 At Failure	79
4.32	Stresses and Total Force in Longitudinal Bars (Specimen C2).	80
4.33	Specimen C2 Principal Surface Strain	81
4.34	Specimen D1 Crack Pattern.	83
4.35	Specimen D1 At Failure	84
4.36	Stresses and Total Force in Longitudinal Bars (Specimen D1).	85
4.37	Specimen D1 Principal Surface Strain	86

4.38	Specimen D2 Crack Pattern.	88
4.39	Specimen D2 At Failure	89
4.40	Stresses and Total Force in Longitudinal Bars (Specimen D2).	90
4.41	Specimen D2 Principal Surface Strain	91
5.51	Node Effective Dimensions.	95
5.2	Specimen A1 Effective Dimensions	95
5.3	Specimen with Anchorage Failure: Ratio of Total Bar Force at Failure (F_y) to Yield Load (F_y)	106

CHAPTER 1

INTRODUCTION

1.1 General

A proper design of concrete members having geometric discontinuities (corbels, joints, openings, deep beams...) requires the use of lengthy methods of analysis or the use of empirical procedure that have the inconvenience of being applicable to specific situations only. In addition the detailing of the reinforcement in structural concrete is usually not performed in a systematic way. The Strut and Tie Model is based on theory of plasticity and provides the engineer with a systematic load path method for the design and detailing of structural concrete.

1.2 Background

The concept of an analogy to a truss for the behavior of structural concrete was first introduced by Ritter (16) and Mörch (13) near the turn of the century. Theoretical aspects of this method were extensively investigated (8,11,12,17). Schlaich et al. (17) expanded the strut and tie model to cover entire structures and all concrete structures. However experimental research was performed with this model was limited in scope.

In this model the structural element is replaced by an

analogous truss system as explained with the simple example of a beam with a vertical point load (Fig.1.1). The compressed concrete simulates the truss top chord, the tensile reinforcement simulates the lower chord. The transverse reinforcement represents the vertical hangers. Compressed concrete struts act as the truss diagonals. The nodes represent the intersection of struts and ties and imply an abrupt change in the direction of the forces. The application of the strut and tie model can be extended to any type of structure (Fig.1.2).

Designing a structure using the strut and tie model involves the selection of an appropriate model to distribute the forces, the determination of the forces in the ties and the struts by satisfying the internal equilibrium (using truss analysis), and the dimensioning of the elements of the model (ties, struts, and nodes). The tie forces are resisted by tensile reinforcement, the stresses in the strut are checked and the nodes are dimensioned to insure a proper anchorage of the tie and a transfer of the forces.

To provide a better understanding of the behavior of the node in a strut and tie model, Barton (3) conducted experimental work at the University of Texas at Austin on a dapped beam (Fig.1.3). Comparison between experimental data, analysis, and the crack pattern at failure (Fig.1.4) showed that the strut and tie

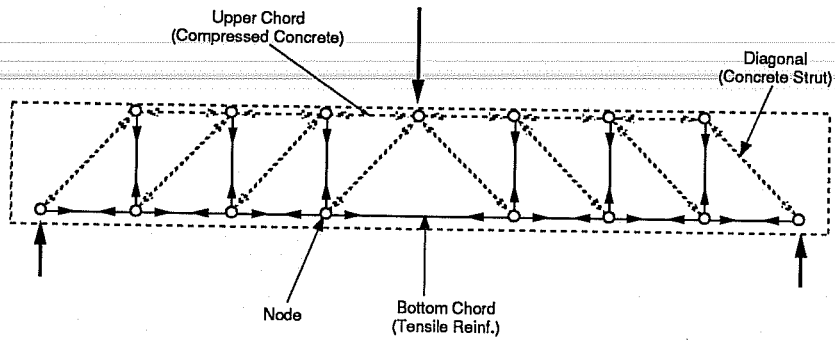
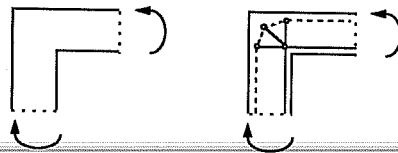
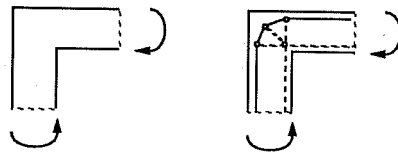


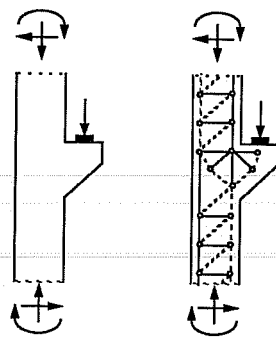
Fig 1.1 Strut and Tie Model for a Beam



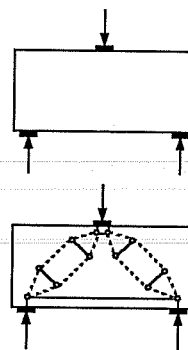
(a) Moment Opening Corner



(b) Moment Closing Corner



(c) Corbel



(d) Deep Beam

Fig. 1.2. Examples of Strut and Tie Models
(From Ref. 17)

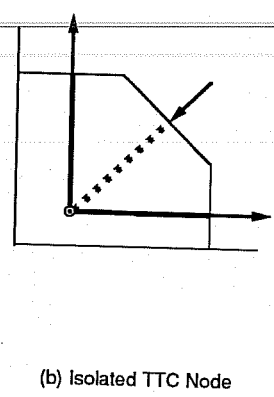
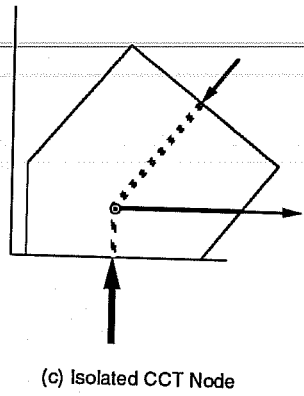
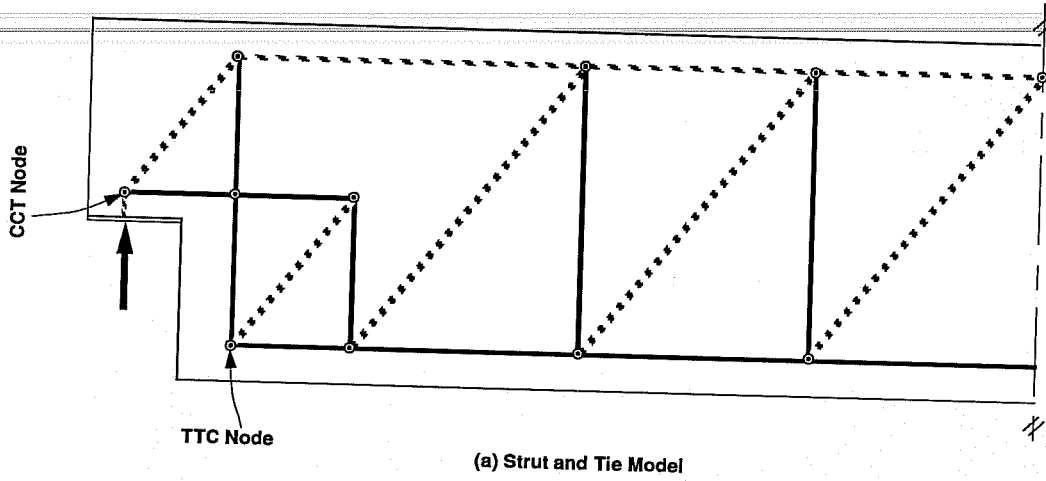


Fig 1.3 Strut and Tie Model of the prototype Dapped Beam

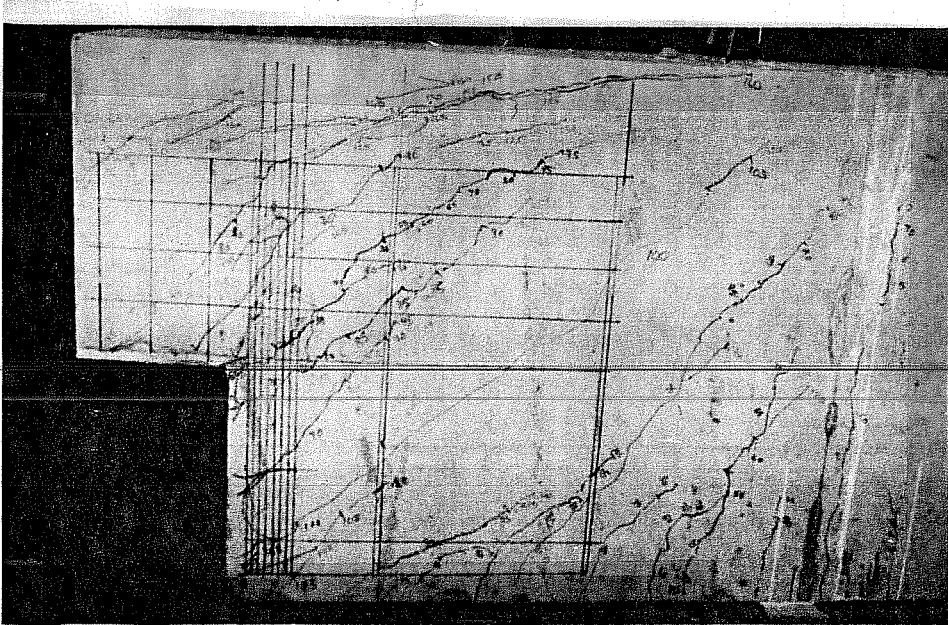


Fig. 1.4 Prototype Dapped Beam Crack Pattern
(From Ref. 3)

model is an efficient and appropriate detailing and design method in structural concrete.

Anderson (2) isolated and tested a Tension-Tension-Compression (TTC) node (Fig.1.3b) in a subsequent experimental program. This study helped in developing a behavioral pattern for the TTC node and determining the dimensions of the node and the strut inclination.

1.3 Objectives of the Study

For the study reported here the Compression-Compression-Tension (CCT) node located at the reaction area of the dapped beam was isolated and tested (Fig.1.3c). The design and behavior of the CCT node is influenced by:

1. Proper sizing of the node: the primary step in designing the node is the determination of the dimensions. Different methods (12,18) have been proposed, however none was experimentally verified.

2. Concrete stresses: the concrete strut stresses (f_c) have to be kept below a safe level at the node boundaries. Analytical models define the safe level of stresses in the following form:

$$f_c = \nu f'_c$$

where

ν is the efficiency factor.

f'_c is the concrete compressive strength

Numerous expressions have been proposed for ν but none experimentally justified for a CCT node.

3. Reinforcement: The reinforcement should be able to develop the tie force. The location, arrangement, and diameter of the bars influence the size of the node and the bearing pressure as demonstrated in Figure 1.5.

4. Lateral confinement by transverse reinforcement: The transverse reinforcement can improve node behavior by arresting the cracks growth and by confining the concrete.

5. Anchorage of the tie. To function properly the tie needs to be anchored in the node. However little guidance exists for determining the point at which anchorage starts. Hooks may improve anchorage of the tie.

The purpose of this experimental study is to provide an understanding of the behavior of the CCT node by examining the effect of the parameters listed above.

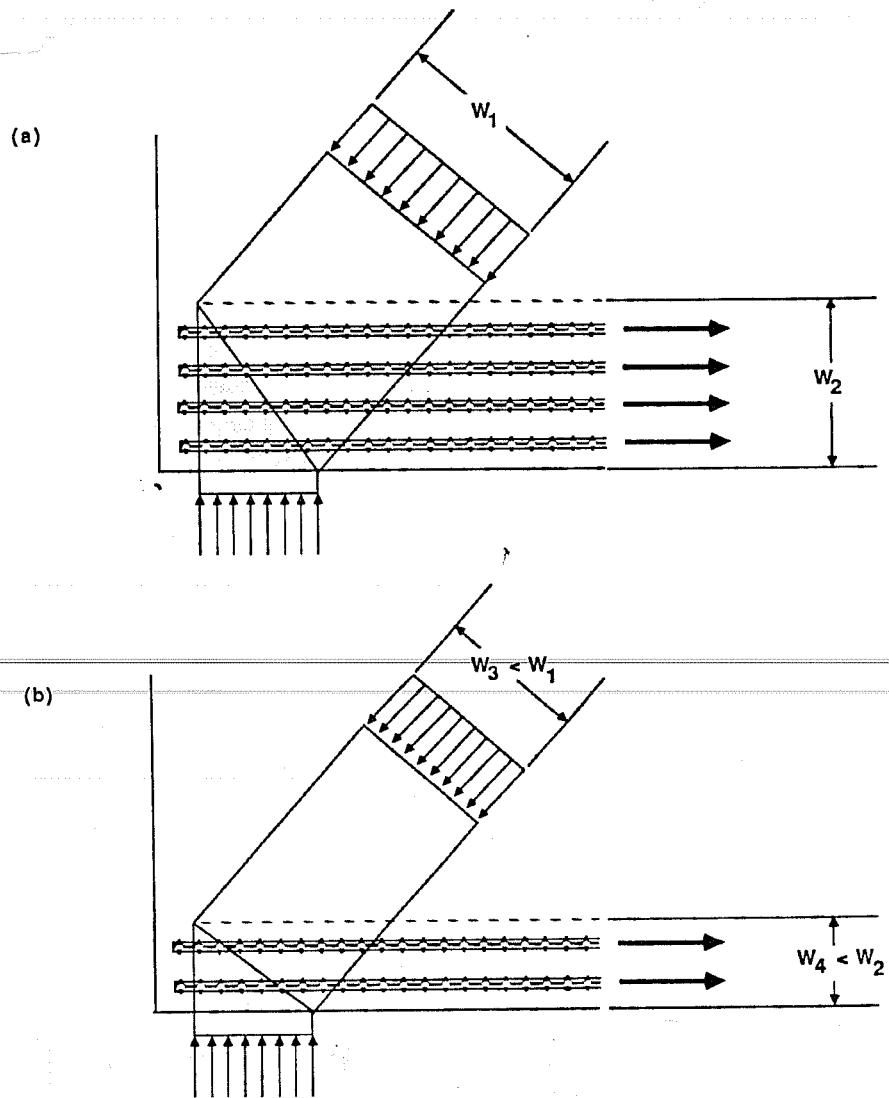


Fig. 1.5 Effect of Reinforcement Layout on Node Dimensions
(From Ref. 2)

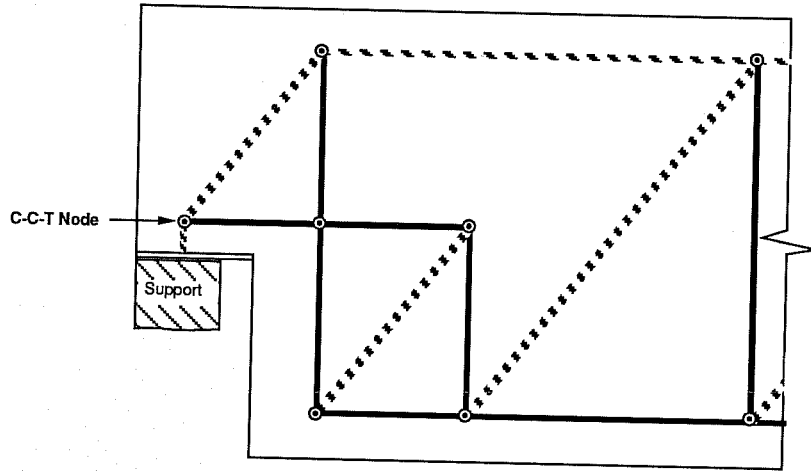
CHAPTER 2

SPECIMEN DETAILS

2.2 Geometry of the Test Specimens

The C.C.T node located at the support of in prototype dapped beam previously tested by Barton (3) was isolated and tested in this study (Fig.2.1). A review of the available work (12,17) shows that node regions are difficult to define. Boundaries and strut inclinations cannot be defined uniquely. The proportions of the node used in this study were based on the recommendations of Schlaich et. al. (17). Furthermore, the results of an elastic stress analysis (Fig.2.2) showed that the node is a disturbed region in which the stress trajectories do not have well defined angles. The strut angle for the specimens tested (Fig.2.3) was the same as that in the strut and tie model used in designing the prototype dapped beam.

The dimensions and the shape of all the specimens were the same. The reinforcement layout was based on the original beam. However in order to estimate the resistance of the strut a larger reinforcement area was used so that concrete crushing would control the mode of failure.



(a) Strut-and Tie Model and Location of the C-C-T Node

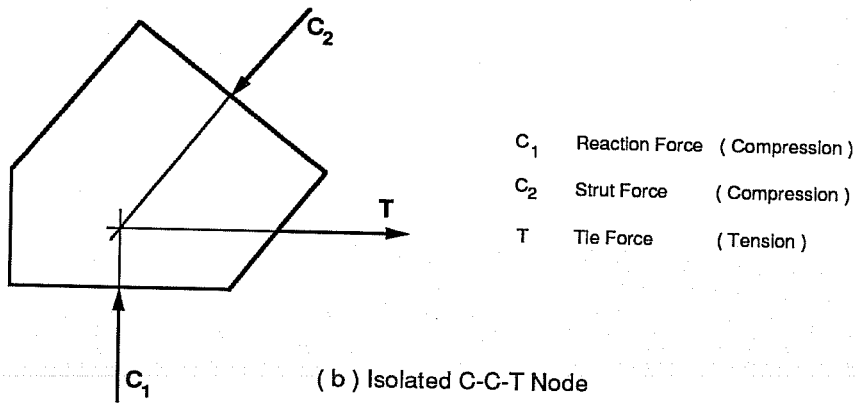
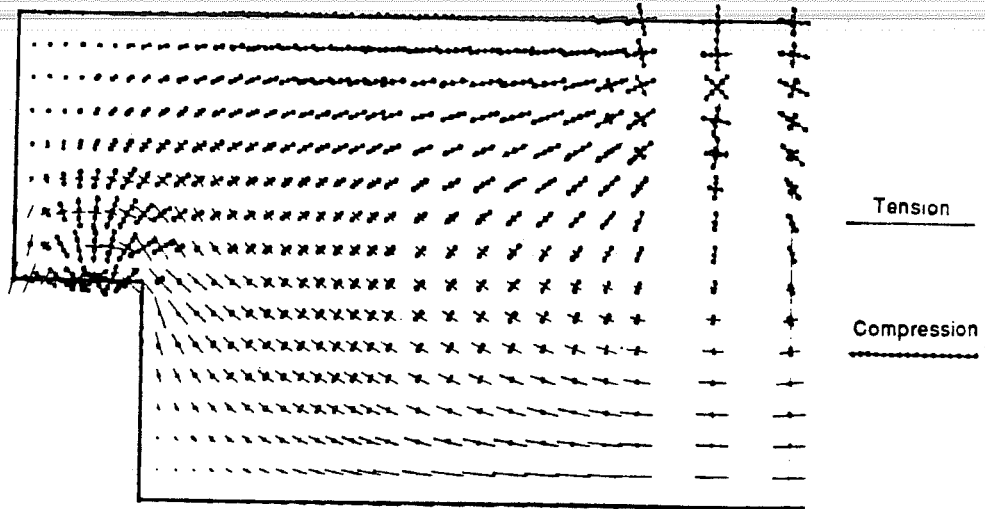


Fig. 2.1 Original Dapped Beam

(a)



(b)

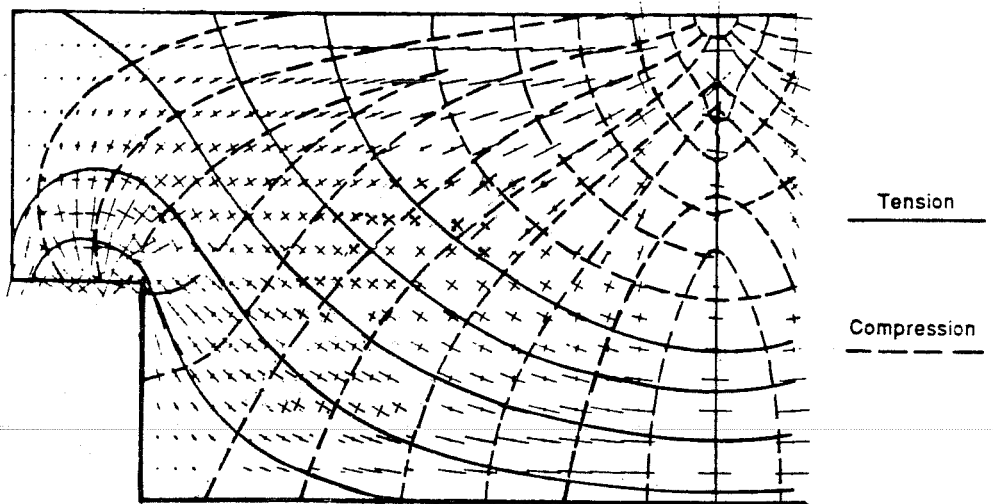
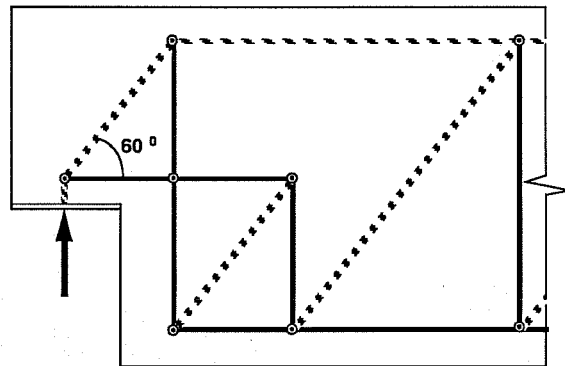
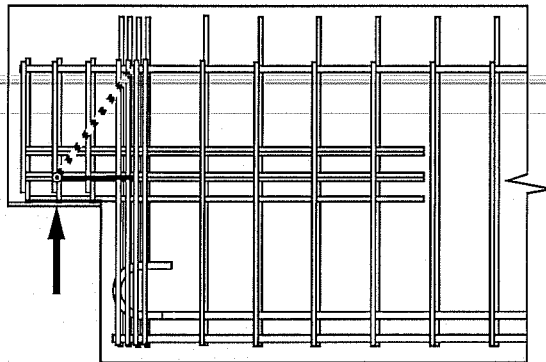


Fig 2.2 Stress Trajectories
(From Ref. 2)



(a) Strut and Tie Model



(b) Reinforcement

Fig 2.3 Strut Angle of the CCT Node Investigated

2.3 Specimen Details

Two series of tests were performed. In each series a different set of parameters was investigated. In Series I, the compressive strength of the node for a given longitudinal reinforcement layout was considered. Series II investigated the effect of different longitudinal reinforcement layouts on node behavior.

In series I, five tests (A1, B1, A2, B2 and A1-R) were performed in order to evaluate the effect of the support size and the confinement condition on the compressive strength of the concrete. The dimensions and longitudinal reinforcement are shown in Figure 2.4. Specimen A1 and A2 were confined with #3 transverse ties (Fig.2.5a), while specimen B1 and B2 were not confined (Fig.2.5b). Comparisons between those two specimen were intended to show the effect of confinement on node behavior. In order to evaluate the effect of the support size and the strut size on the performance of the node, two loading plate widths were used. In specimen A1 and B1 a full width support plate was used (Fig.2.6a). In Specimen A2 and B2 a half width support plate was used (Fig.2.6b).

The details of Series I specimens are summarized in Table 2.1.

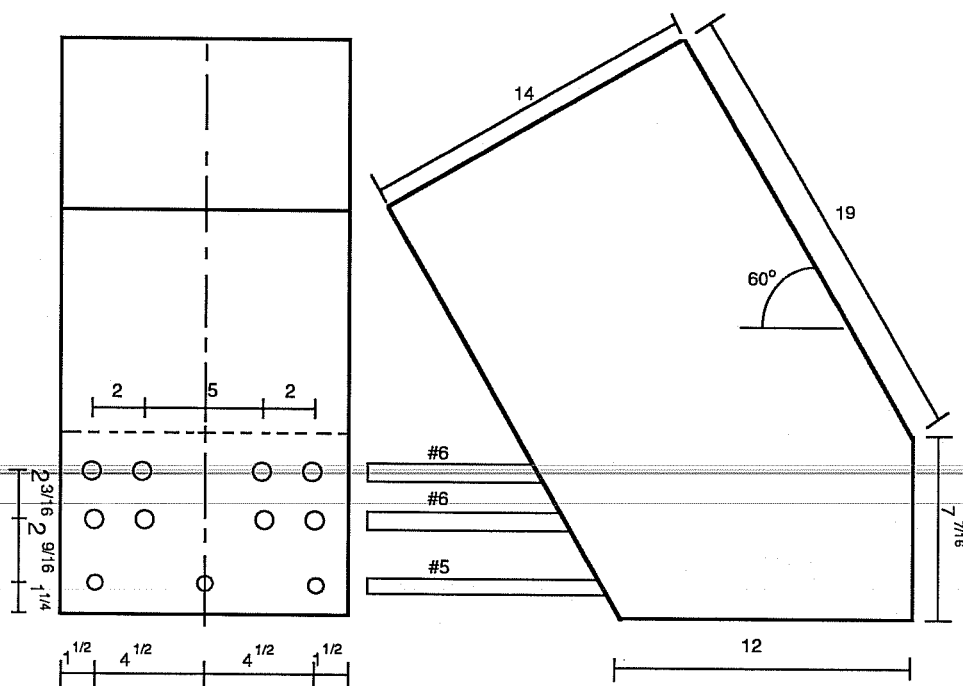
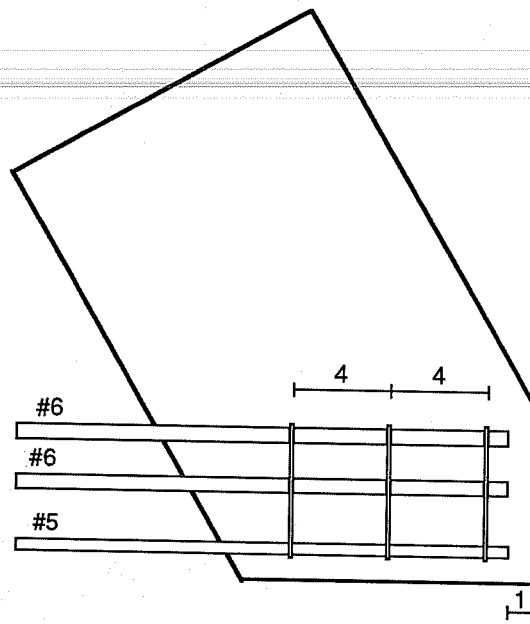
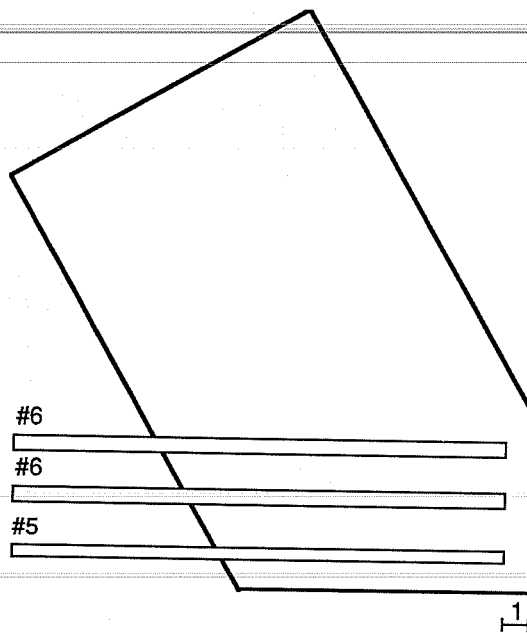


Fig. 2.4 Series I Details (Specimens A1, B1, A2, B2, A1-R)

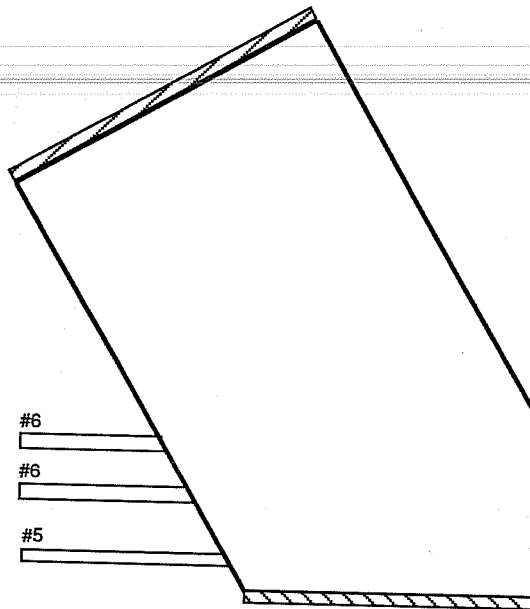


(a) Specimen A1, A2 and A1-R

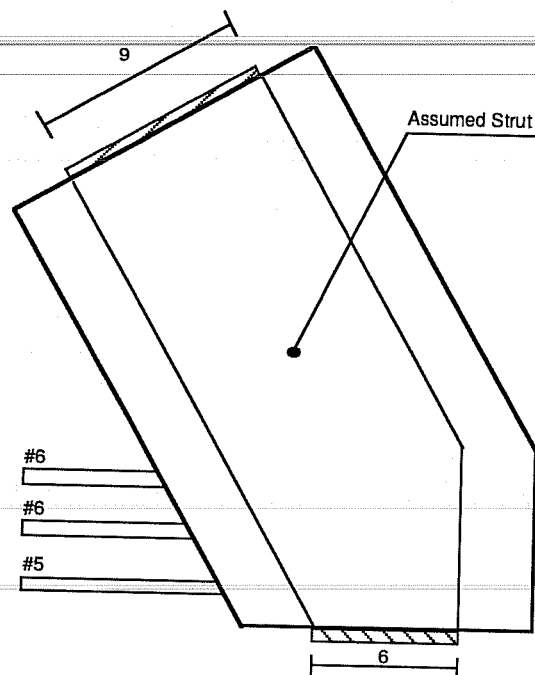


(b) Specimen B1 and B2

Fig. 2.5 Reinforcement Configuration of Series of Specimens



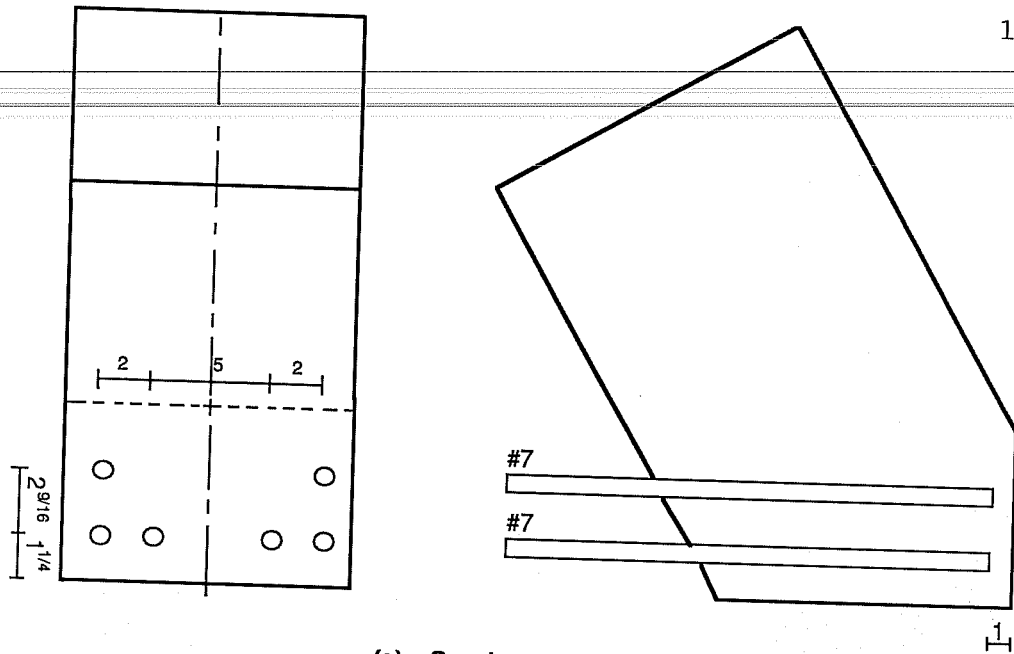
(a) Full Width Loading Plates Used for Node Specimen A1, B1 and A1-R



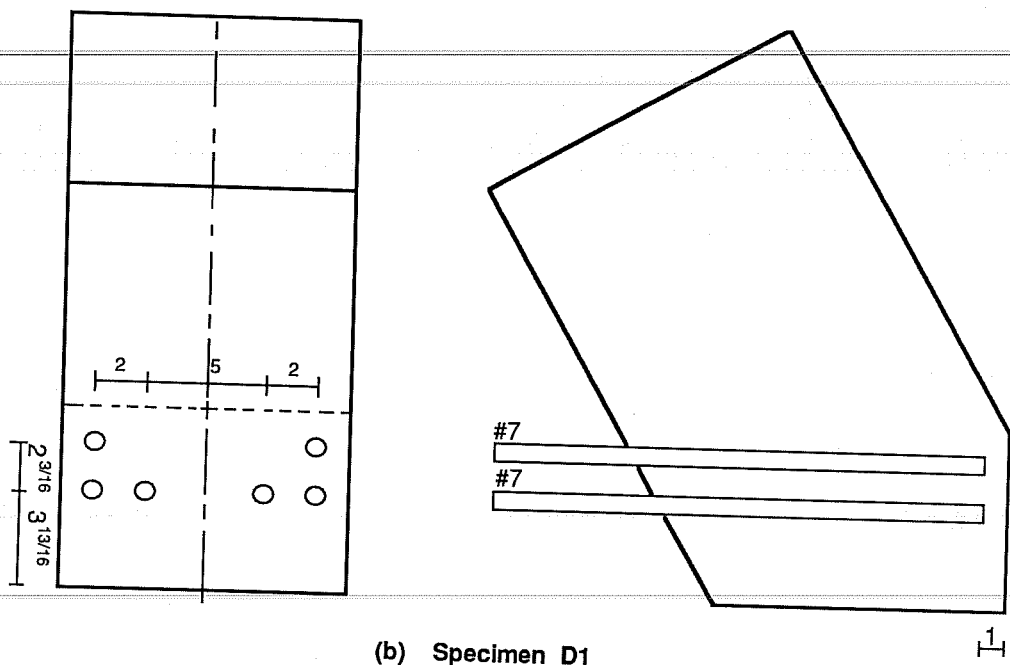
(b) Half Width Loading Plates Used for Node Specimen A2 and B2

Fig 2.6 Bearing Areas, Series I

In Series II, which included five tests (A1-2, C1, D1, C2, D2), the effect of the reinforcement layout on node resistance was studied. Specimen A1-2 (Fig.2.4) was a duplicate of specimen A1 of Series I to help make comparisons between the two series. The other specimens had different reinforcement layouts while the total steel area was kept constant. However the location of the reinforcement and the use of hooks on some bars provided means of examining the anchorage conditions. Specimens were designed either with a bar cover of 7/8 in. from the bottom edge of the specimen or a cover of 3 in. The effect of hooked bars was investigated by providing 180° standard ACI hooks in two specimens. Figures 2.7a through 2.7d give the details of specimens C1, D1, C2 and D2. The details of series II specimens is summarized in Table 2.2.

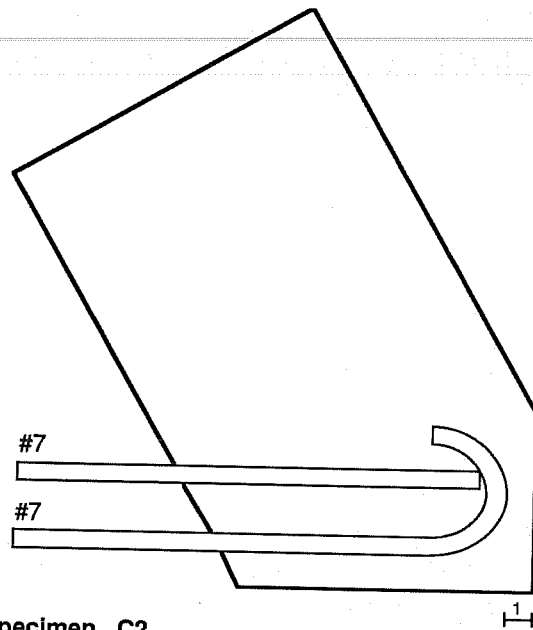
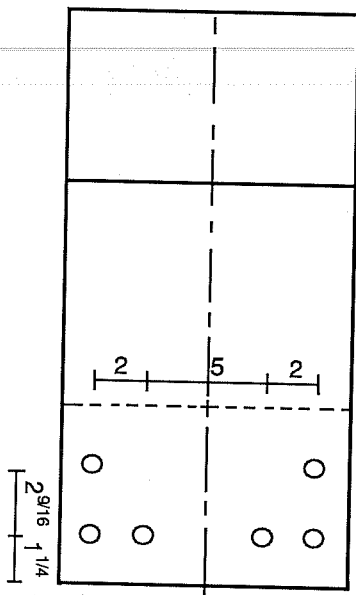


(a) Specimen C1

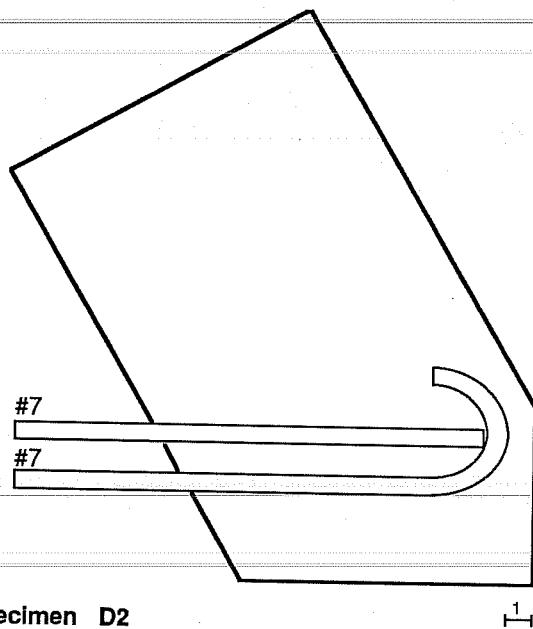
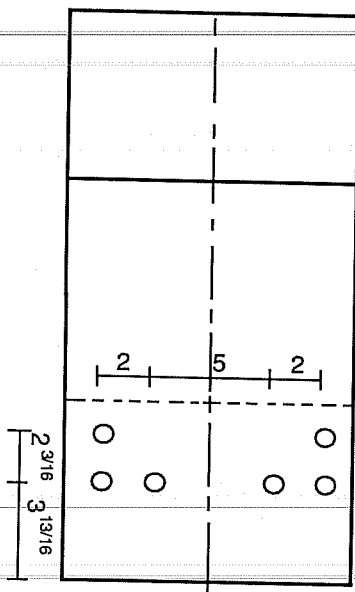


(b) Specimen D1

Fig 2.7 Reinforcement Configuration of Series II



(c) Specimen C2



(d) Specimen D2

Fig 3.7 Reinforcement Configuration of Series II (Continued)

Specimen	f'_c (psi)	Bearing Plate	Rebars Used	Trans. Reinforc.
A1	2340	Full (fig 2.6a)	3 #5, 8 #6 (fig 3.3)	Yes
B1	2470	Full (fig 2.6a)	3 #5, 8 #6 (fig 3.3)	No
A2	2490	Half (fig 2.6b)	3 #5, 8 #6 (fig 3.3)	Yes
B2	2600	Half (fig 2.6b)	3 #5, 8 #6 (fig 3.3)	No
A1-R	2610	Full (fig 2.6a)	3 #5, 8 #6 (fig 3.3)	Yes

Table 2.1 Summary of Series I




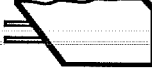

Specimen	f'_c (psi)	Rebars Used	Reinf. Layout	180° Hook
A1-2	4860	3 #5, 8 #6 fig 2.4		N.A.
C1	5005	6 #7 fig 2.7a		No
C2	5015	6 #7 fig 2.7c		Yes
D1	5025	6 #7 fig 2.7b		No
D2	5025	6 #7 fig 2.7d		Yes

Table 2.2 Summary of Series II

CHAPTER 3

EXPERIMENTAL INVESTIGATION

3.1 Materials

3.1.1 Concrete. The specimens were cast using ready mix concrete with type I Portland cement, washed Colorado River sand and 3/8 in. coarse aggregate for Series I and 3/4 in. for Series II. Tables 3.1 and 3.2 summarize the mix proportions. Six by twelve cylinders were tested at 7 days, 14 days and 28 days to obtain the strength versus time curve. Three cylinders were tested at each age. Tests were also performed when a specimen was tested. The values obtained are summarized in Table 3.3. Strength-Time curves are shown in Figures 3.1 and 3.2.

3.1.2 Reinforcing Steel. Standard ASTM-A615 deformed reinforcing bars were used for all specimens. Grade 60 #5 and #6 straight longitudinal bars and #3 transverse bars were used in Series I. Grade 60 #7 bars were used in Series II. Straight and hooked longitudinal bars were used in Series II. ACI 318 standard 180° hooks were used for the bends.

Tensile tests were performed on each group of bars to obtain the stress-strain relationship. Two coupons were cut from

Materials	Amount (per cu. yd.)
Coarse Aggregates	1920 lbs
Fine Aggregates	1467 lbs
Cement	347 lbs
Water	156 lbs (19 gals)

Water / Cement Ratio (by Weight) = .45

Cement factor = 3.7 sack/cu. yd.

Slump = 3 in.

Table 3.1 Concrete Mix Design for Series I
(A1, B1, A2, B2, A1-R)

Materials	Amount (per cu. yd.)
Coarse Aggregates	1633 lbs
Fine Aggregates	1527 lbs
Cement	380 lbs
Water	78 lbs (9.4 gals)

Water / Cement Ratio (by Weight) = .21

Cement factor = 4.04 sack/cu. yd.

Slump = 3 in.

Table 3.2 Concrete Mix Design for Series II
(A1-2, C1, D1, C2, D2)

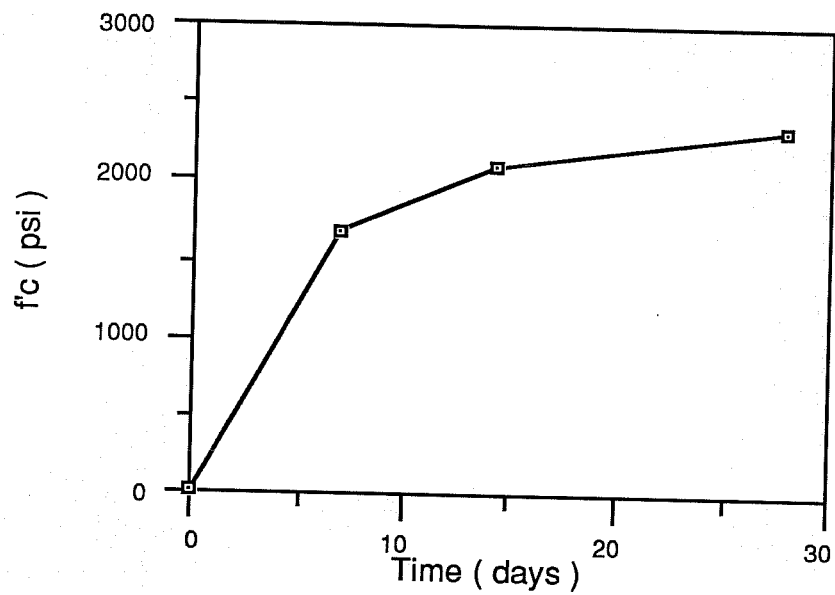


Fig. 3.1 Concrete Strength vs. Time Curve for Concrete in Series I (A1, A2, B1, B2, A1-R)

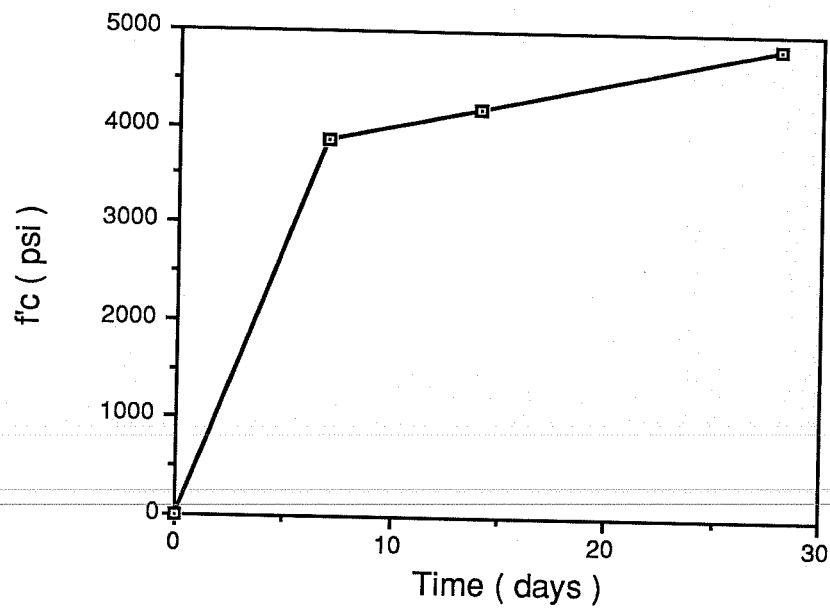


Fig. 3.2 Concrete Strength vs. Time Curve for Concrete in Series II (A1-2, C1, D1, C2, D2)

each heat. An 8in. extensometer was used to monitor the strain. The stress-strain curve was plotted during the test. Figures 3.3 through 3.6 show those plots. The properties of the bars are summarized in Table 3.4.

3.2 Instrumentation

3.2.1 Strain Gages. The strains were monitored with strain gages mounted on all longitudinal bars and transverse hoops. Gages were mounted on the longitudinal reinforcement 2.5 in. from the concrete face. The location of the gages are shown in Figure 3.7.

3.2.2 Linear Potentiometer. Potentiometers were used to monitor the deflections. A 10 in. potentiometer mounted on the loading machine gave the vertical deflection of the test machine head. The potentiometer (Fig.3.8) was located behind the outer bars and could give an indication of slip between the bars and the concrete.

3.4.3 Demec Gage Readings. Demec points were used to measure the surface strain. The Demec points were placed in a pattern to provide a 2 in. gage length. The Demec points covered a large surface of the first specimen tested (Specimen A1) (Fig.3.9a) and were used to measure the strain along lines that were expected to be principal directions. The data showed that the

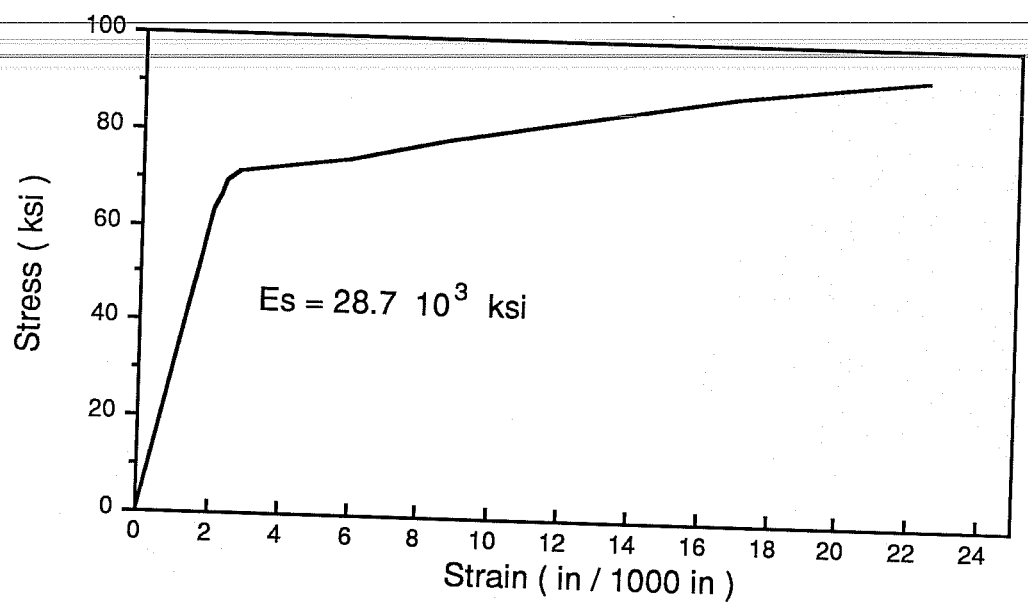


Fig 3.3 Strain-Stress Curve for #3 Grade 60 Reinforcement Bar

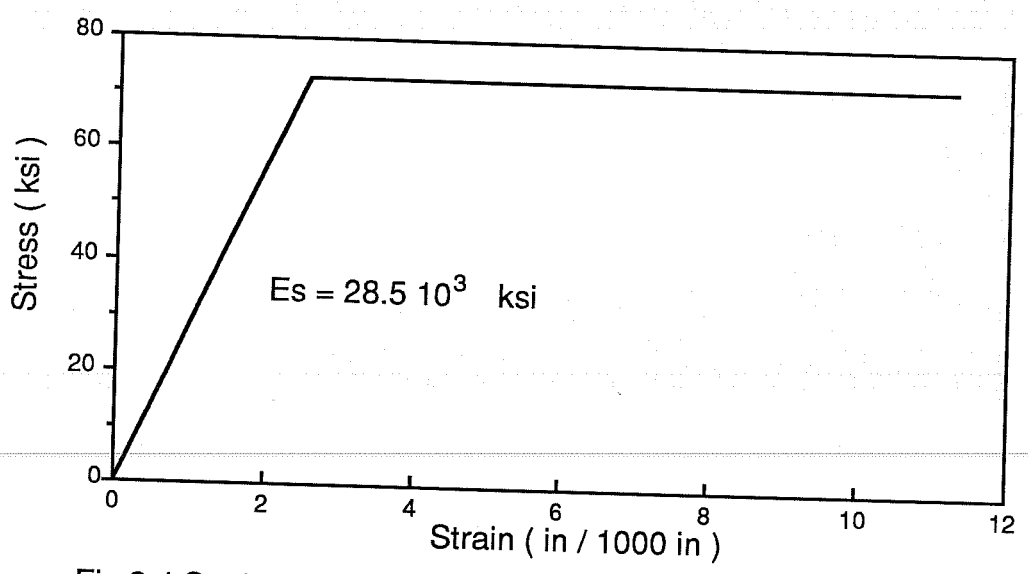


Fig 3.4 Strain-Stress Curve for #5 Grade 60 Reinforcement Bar

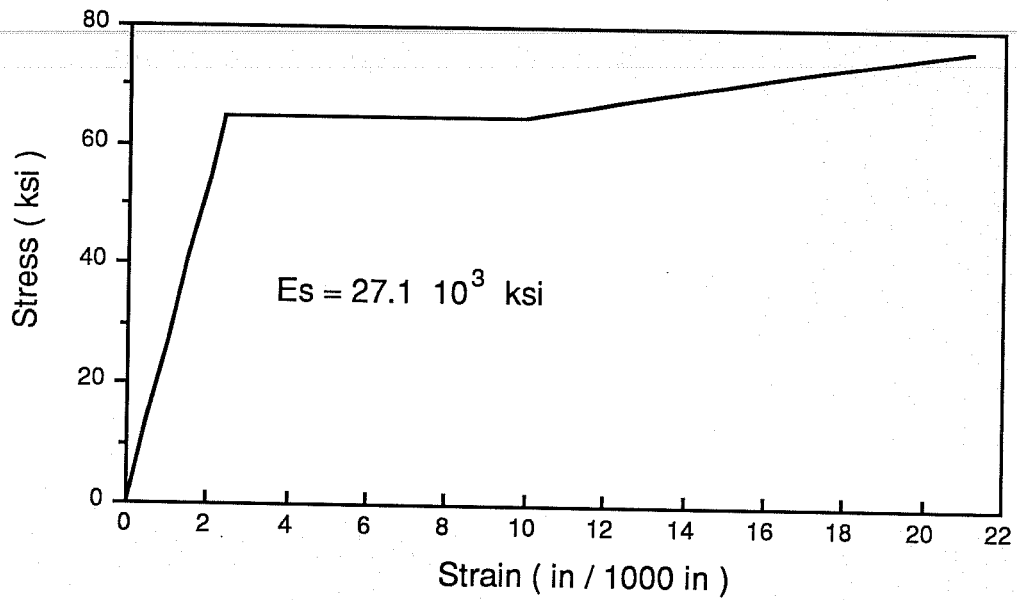


Fig. 3.5 Strain-Stress Curve for #6 Grade 60 Reinforcement Bar

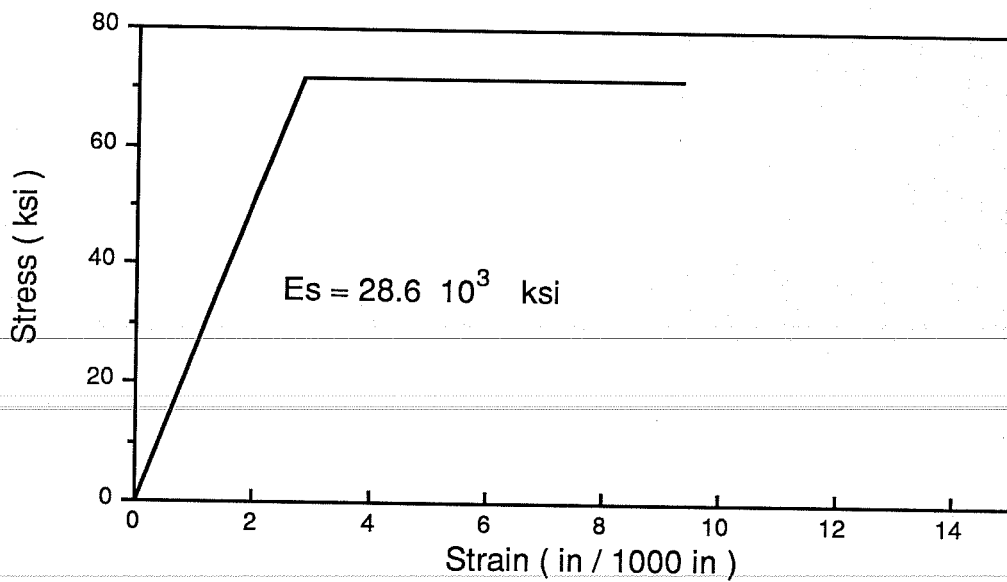


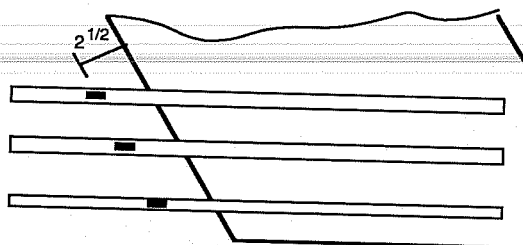
Fig. 3.6 Strain-Stress Curve for #7 Grade 60 Reinforcement Bar

Time (days)	Concrete Strength (psi)	
	Series I	Series II
7	1690	3865
14	2115	4200
28	2360	4860

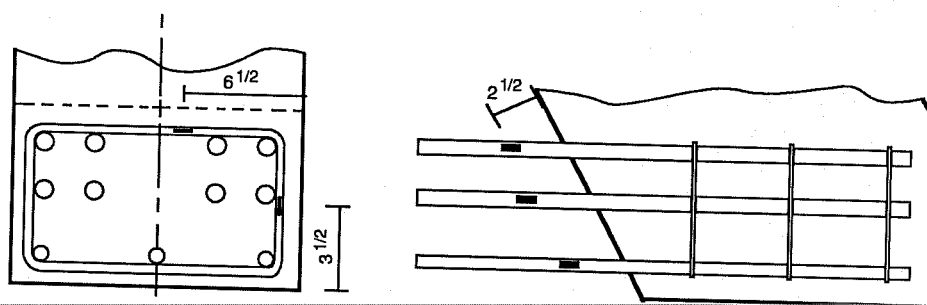
Table 3.3 Concrete Strength

Rebar #	3	5	6	7
Modulus of Elasticity (10^3 ksi)	31.0	28.5	27.1	28.6
Yield Strength (ksi)	71.3	72.7	64.8	71.7

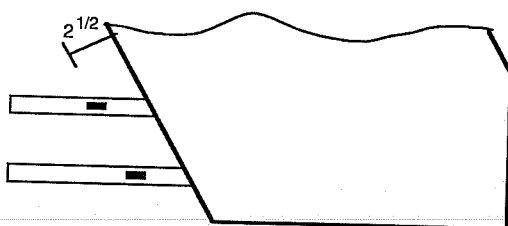
Table 3.4 Reinforcement Properties



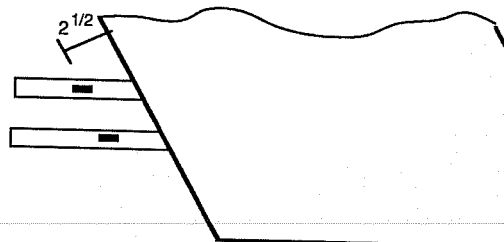
(a) Specimen B1 and B2



(b) Specimen A1, A2, A1-2 and A1-R



(c) Specimen C1 and C2



(d) Specimen D1 and D2

Fig. 3.7 Strain Gage Location

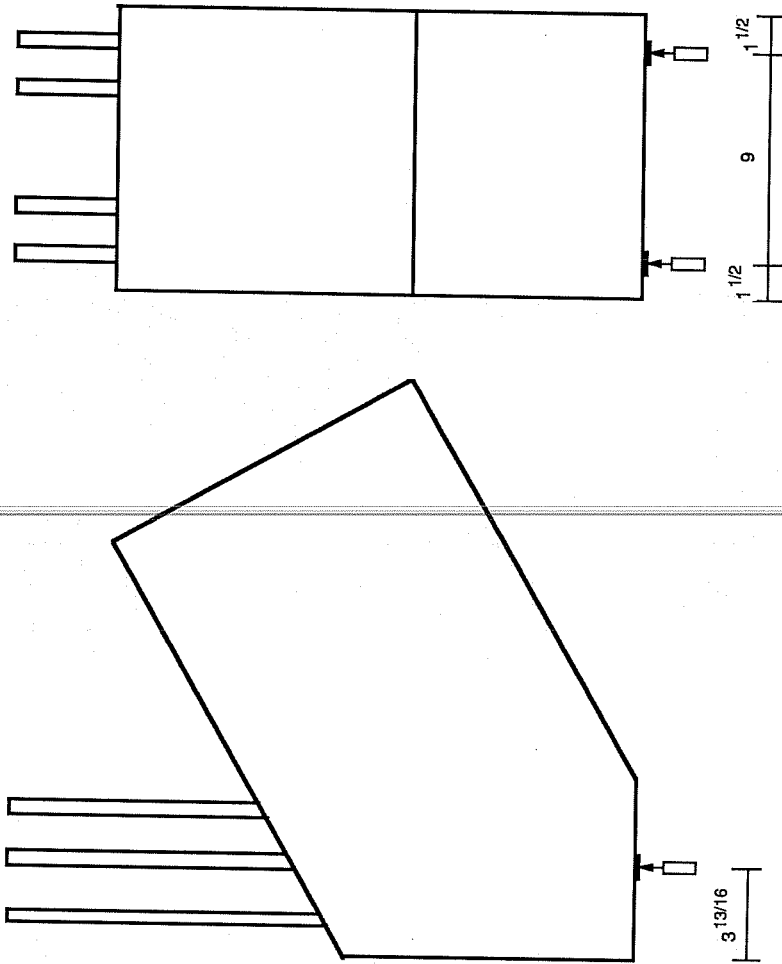
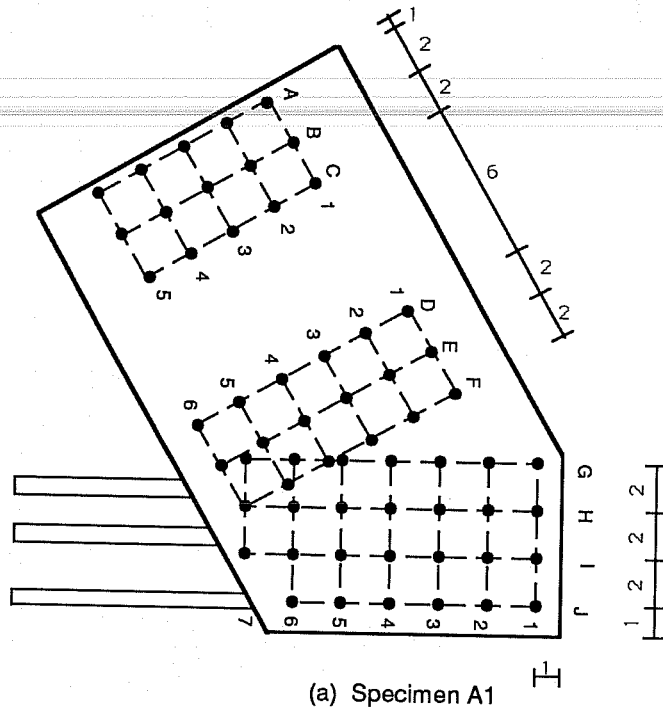
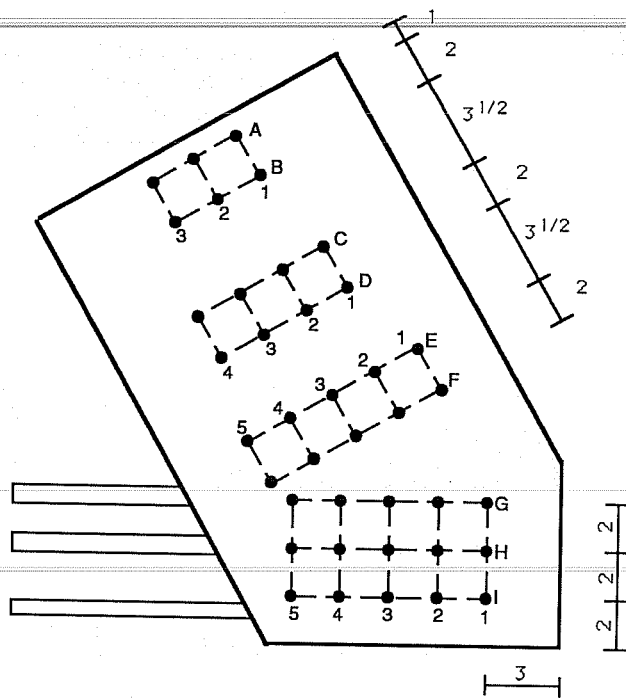


Fig 3.8 Linear Potentiometer Location

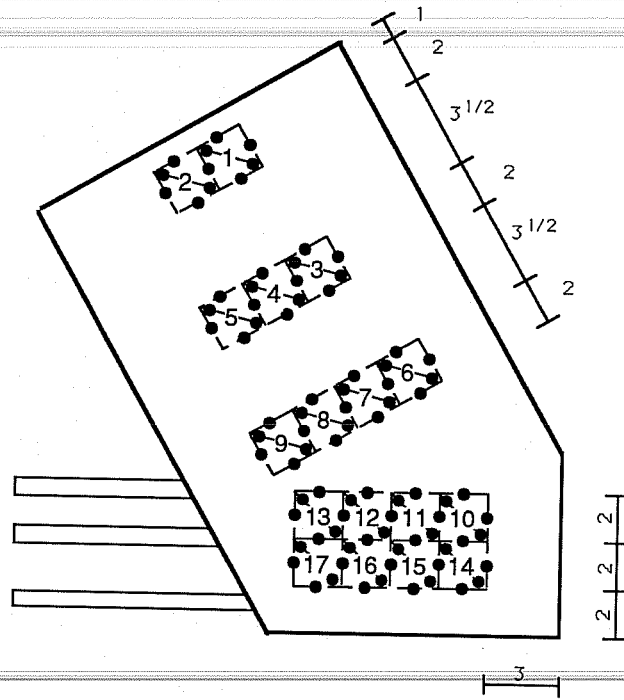


(a) Specimen A1



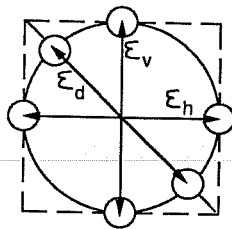
(b) Specimen A2 and B1

Fig. 3.9 Location of Demec Points for Surface Strain Measurements



(c) Remaining Specimen
(B2, A1-R, A1-2, C1, C2, D1, D2)

Example of a Station Reading



- ϵ_h Strain Reading In the Horizontal Direction
- ϵ_v Strain Reading In the Vertical Direction
- ϵ_d Strain Reading In the Diagonal Direction

Fig. 3.9 Location of Demec Points for Surface Strain Measurements (Continued)

points located near the edge of the specimen did not give any important information. Thus, the number of points were reduced for specimens B1 and A2 (Fig.3.9b). The data for specimens A1, A2, and B1 indicated that the directions selected were not principal directions. Thus, a strain rosette was used for the remaining specimens (Fig.3.9c). Such a rosette permitted computing the principal directions and principal strains.

3.3 Specimen Fabrication

Because the small size of the specimen reduced the tolerance, attention was given to the dimensioning and fabrication of the forms. Thus, special care was taken to maintain the angles and dimensions. The inside faces of the forms were sanded to remove the irregularities and lacquered to reduce water absorption and to make removal easier. Forms are shown in Figure 3.10.

The longitudinal reinforcement passed through a predrilled form and was supported by an additional template. The template was positioned with respect to the forms to insure correct location of the bars. In specimens with transverse reinforcement, the hoops were placed after the longitudinal bars were positioned.

While internal strain gages were mounted before casting, external strain gages were mounted after the forms were removed.

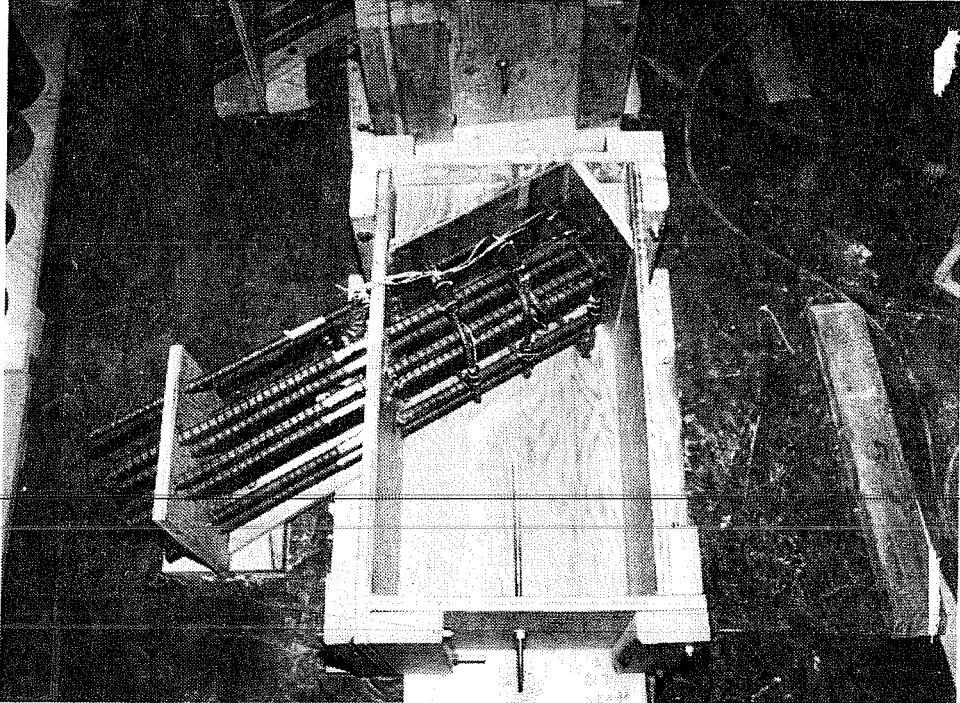


Fig. 3.10 Steel Cage and Formwork

The internal gages were protected with a water proof barrier. An insulating material and a neoprene rubber pad protected the gages during concrete placement and vibration.

Ready mix concrete was used to cast the specimen. Slump tests were taken prior to casting. Water was added to obtain the correct slump. Concrete was consolidated using a flexible shaft internal vibrator. 6 in. by 12 in. cylinders were cast with the specimens.

Approximately three hours after casting, the specimen and the cylinders were covered to provide good curing conditions and to avoid possible differential shrinkage. Moist burlap was used to cover the specimens.

The forms were removed two days after casting. The forms were easily removed with the exception of the front form (the template for bar location) which was destroyed because the inclined bars passing through it made removal impossible. Cylinders were removed from the molds on the same day.

3.4 Experimental Setup

The specimen was placed in a setup which is shown in Figure 3.11. Stiffeners welded to the web carried the load directly to the test machine. The top element of the setup consisted of welded steel plates (bolted to the support beam)

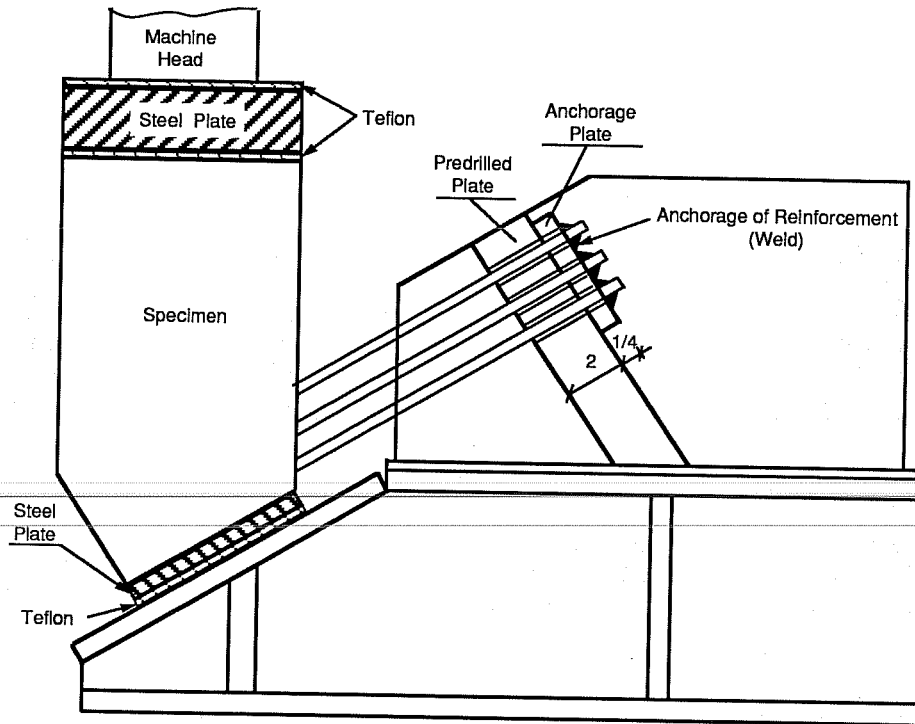


Fig 3.11 Elevation of Test Setup

which provided a bulkhead to anchor the protruding bars.

3.5 Test Procedure

3.5.1. Preparation for testing. The specimen was carefully placed on the support beam. The bars were passed through the predrilled plate. During this process, special care was taken to insure proper positioning of the specimen. After horizontal and vertical alignments were checked, the bars were welded to the anchor plate on the bulkhead (Fig.3.11).

Good bearing surfaces were provided by using hydrostone placed between the specimen and the bottom support plate to produce a uniform bearing surface. The plate had a thickness of 1/2 in. A sheet of teflon was placed between the bottom support plate and the inclined support to avoid the development of frictional forces. A thin layer of hydrostone was cast on the top part of the specimen to obtain a uniform loading surface. A sheet of teflon was placed on the hydrostone layer and a supporting plate was placed on top of the teflon. A sheet of teflon also was inserted between the bearing plate and the machine head (Fig.3.11).

The Demec points were attached to the smooth concrete surface cast against the forms. A grid was first drawn to locate the points which were then glued to the surface using epoxy. The

distance between the points was obtained with the use of a standard 2 in. calibration bar.

The next step involved placing the support beam and the specimen in the machine (Fig.3.12). The test specimen was centered under the machine head. A plumb bob was used to check the correct location of the specimen. Hydrostone was used beneath the support beam to obtain uniform bearing surface between the test machine bed and the beam.

3.5.2 Loading procedure. The loading procedure followed for all specimens involved application of a compressive force to the top surface. Load was increased in 10 kip increment until cracking. The load increment was then reduced to 5 kips until failure.

However, specimen B2 and specimen D2 did not perform well in early stages. The top layer of the reinforcing bars of specimen B2 were in compression or had a low tensile force. When the load reached 275 kips, the specimen was unloaded in order to check a possible bad bearing surface. However no misalignment could be found and the specimen was reloaded until failure.

In the case of specimen D2, cracks at the top of the specimen were noticed at an early stage. These cracks appeared at a load of 200 kips instead of a load of 300 kips as on the other

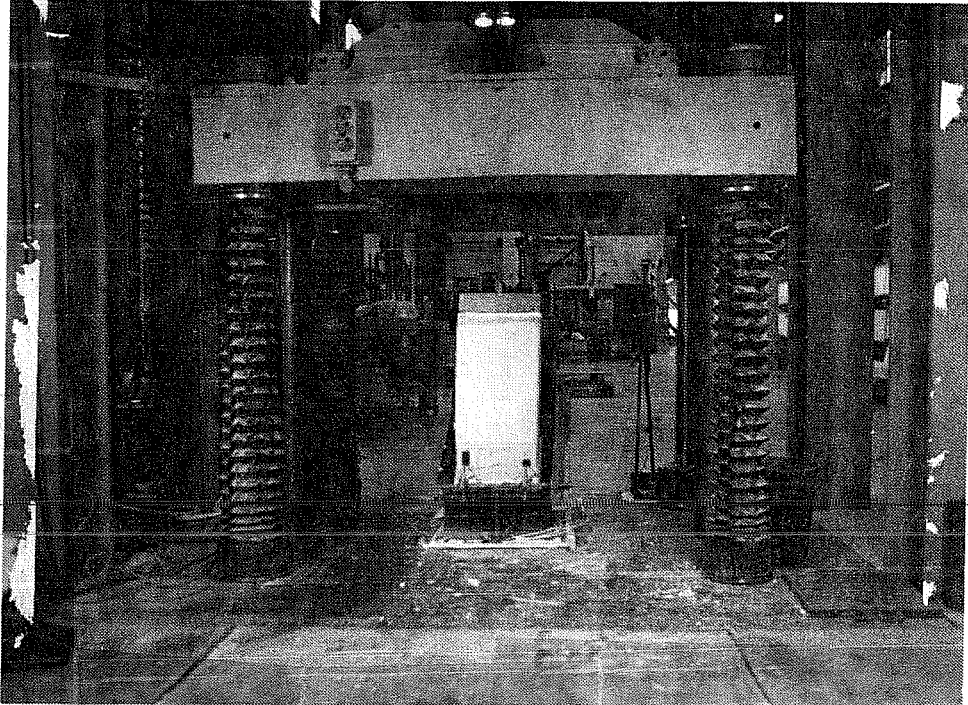


Fig. 3.12 Specimen under the Loading Machine

specimens. When the load reached 275 kips the specimen was unloaded. It was noticed that the bearing plate at the top of the specimen did not have a uniform contact surface. This was corrected by pouring a thin uniform layer of hydrostone between the plate and the specimen. The specimen was then reloaded until failure. While the specimen was being reloaded the cracks closed partially or completely.

3.5.3. Data Collection. Steel strain and potentiometer readings were recorded at every load stage. Surface strains were recorded at selected stages. The pre-crack readings were performed at 50 kip intervals in Series I and every 100 kip interval in Series II. After cracking the readings were taken at selected stages.

Cracks were marked and maximum width of the cracks was noted alongside the trace. Photographs of the cracks were taken at selected stages.

CHAPTER 4
EXPERIMENTAL RESULTS

4.1 Results Presented

Data for each specimen are presented to show trends in behavior and to help explain differences in performance. The following data are presented for each specimen:

1. Longitudinal reinforcing bar stresses. The stresses on individual bars for each reinforcement layer are plotted against the applied load. The cumulative measured force in the bars, the computed force based on the load applied and the geometry of the specimen and the difference between measured and computed bar force (attributed to friction) are compared.

The bar strain readings were influenced by bending in the longitudinal bars caused by a mispositioning of the bars in the forms or by an uneven bearing of the anchorage plate. Consequently, the bar stress distribution was not uniform.

2. Concrete surface strain immediately preceding failure. Surface tensile and compressive strains provide an indication of the strain trajectory and of the compressive strut width. The precision of the readings using the Demec gages is not always satisfactory.

Readings are dependent on the operator. A slight change in the alignment of the gage can result in a different reading.

3. Crack pattern. Crack pattern are shown for every specimen. The cracks provide a good indication of the type of failure and of the effective strut width. The crack width can help in estimating the strain trajectory. The cracks on both side faces of the specimen were similar, thus only the cracks on one side will be shown.

4. Vertical deflection. The vertical deflection of the specimen was recorded and plotted as a function of the applied compressive load. The curves were similar for all specimens. A typical curve is shown in Figure 4.1. It shows a gradual increase in the slope in the lower load range where the contact between the various elements may not yet be good. A constant slope is noticed after that.

4.2 Individual Specimen Test Results

Specimen A1. Specimen A1 (part of Series I) had full size loading plates. The strength of the concrete compressive strut with transverse reinforcement was investigated. The specimen was loaded through a large plate which had a thickness of 1 in.

The crack pattern and the appearance at failure clearly indicate that the specimen failed in compression at a load of 260

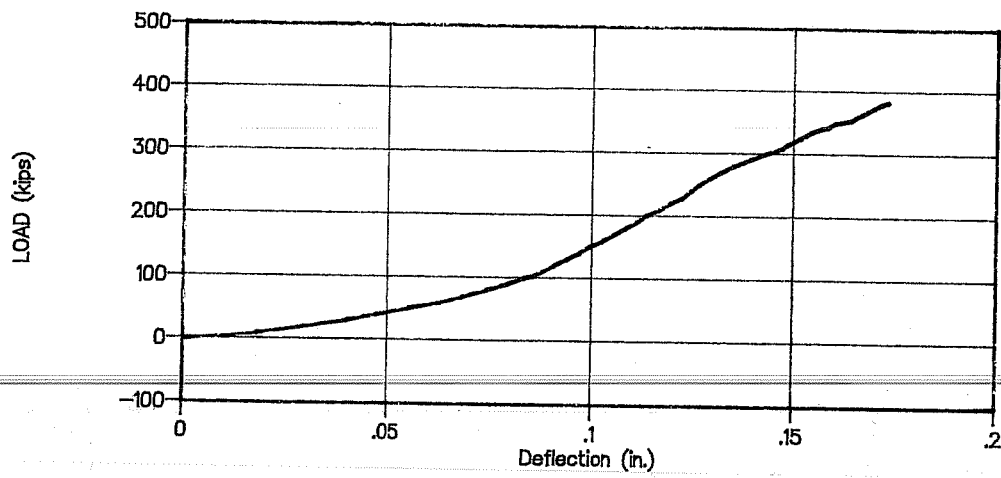


Fig. 4.1 Typical Specimen Load-Vertical Deflection Curve

kips. The first crack appeared on the east side of the specimen at a load of 200 kips. It started from the top and propagated down. The upper part of the crack was parallel to the sides. The crack pattern is shown in Figure 4.2.

At failure the specimen separated into three segments (Fig.4.3a). The central segment may give an indication of the effective strut width. A close look at the appearance of the specimen at failure shows a large shearing crack (Fig.4.3b) which may be due to either poor concrete quality (which was apparent in the test since the failure plane went through the paste and did not fracture the aggregates) or to inadequate thickness (1 in.) of the loading plate. The top loading plate may not have been thick enough to avoid bending and concentration of stress over the central portion of the bearing area. Specimen A1-R which was a duplicate of this specimen (A1) was tested to examine the possibility that uneven stress distribution on the loaded surface produced a premature failure. The size of the top loading plate for the specimen A1-R was doubled (2 in.) to avoid any possible bending.

The stress distribution (Fig.4.4a) in the longitudinal reinforcing bars was not uniform. The lower layer (A) had the highest stresses and the highest stress rate increase. The stresses in the top layer were almost bi-linear. They increased rapidly at

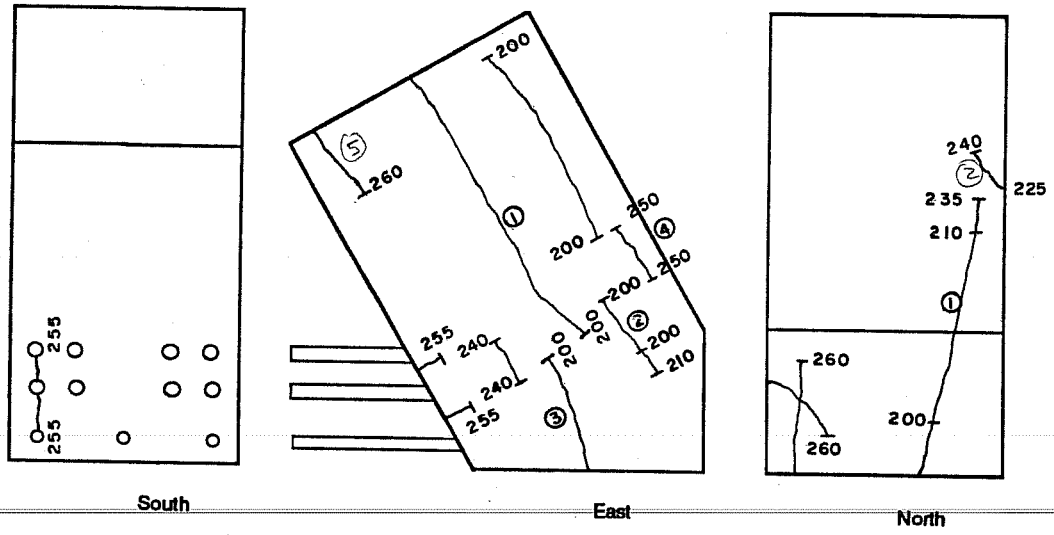


Fig. 4.2 Specimen A1 Crack Pattern

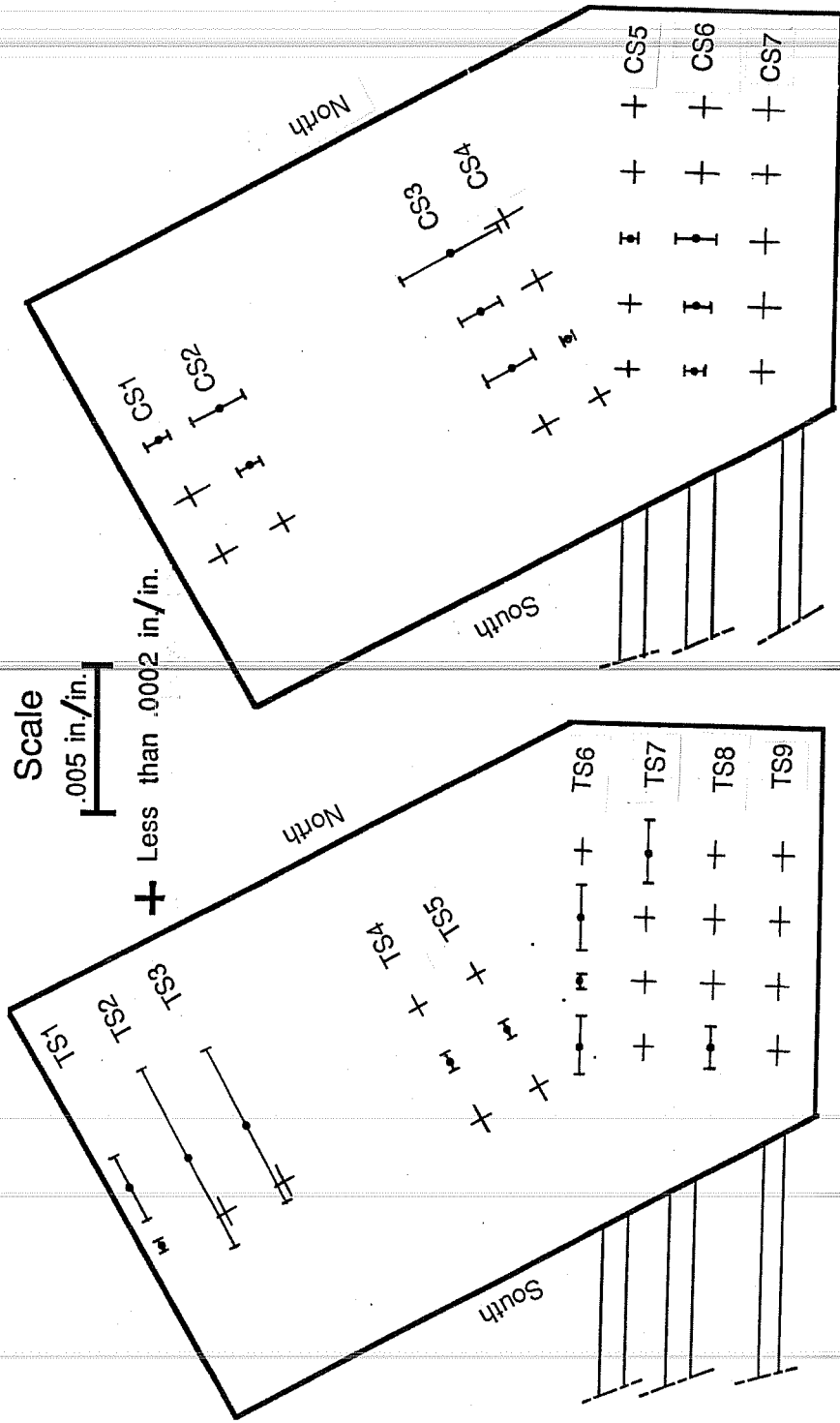
the beginning and then increased at a very low rate. Figure 4.4b shows the bar load.

The surface compressive strains were higher along a line closer to the face of the specimen near the loaded surface (Fig.4.5) and near the middle of the specimen near the bottom support (line CS6). The low value recorded along lines CS4 and CS5 indicate that the gage lines may not have been located on the principal directions. The readings along line CS7 were difficult to make and can be disregarded. High tensile strains coincide with the crack locations.

Specimen B1. In specimen B1 the strength of an unconfined concrete compressive strut was examined.

The first cracks that appeared on the specimen were compressive cracks that developed at a load of 225 kips. They appeared near the loading surface and near the reaction surface (Fig.4.6). The specimen failed in anchorage at a load of 260 kips. Photographs taken at failure (Figure 4.7) indicate loss of cover over the bars near the surface.

The stresses on the longitudinal reinforcement were higher in layer C (top layer). Stresses in layer A (bottom layer) were nearly unchanged throughout the loading (Fig.4.8a). None of the bars



(a) Tensile Strength

(b) Compressive Strength

Fig. 4.5 Specimen A1 Surface Strain (Not Principal)

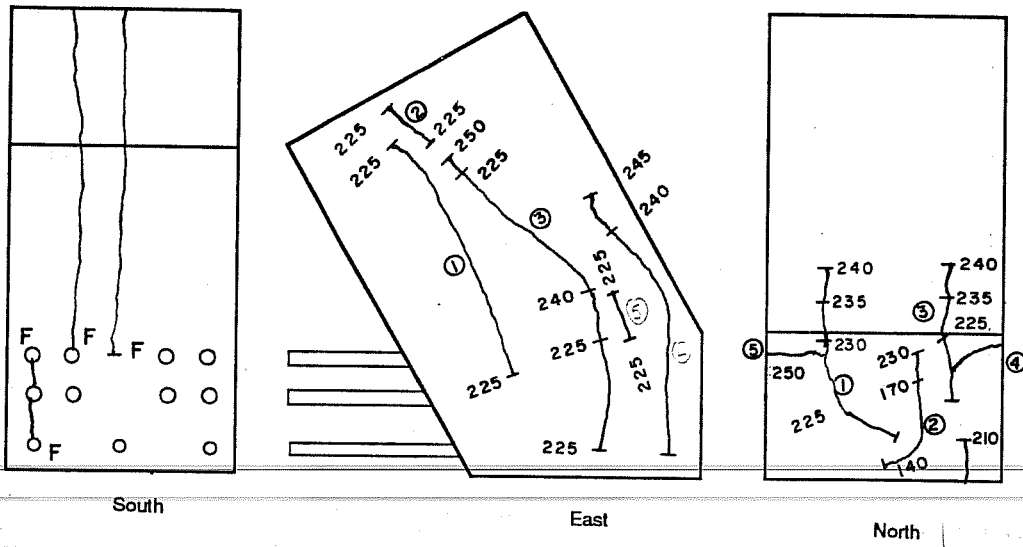
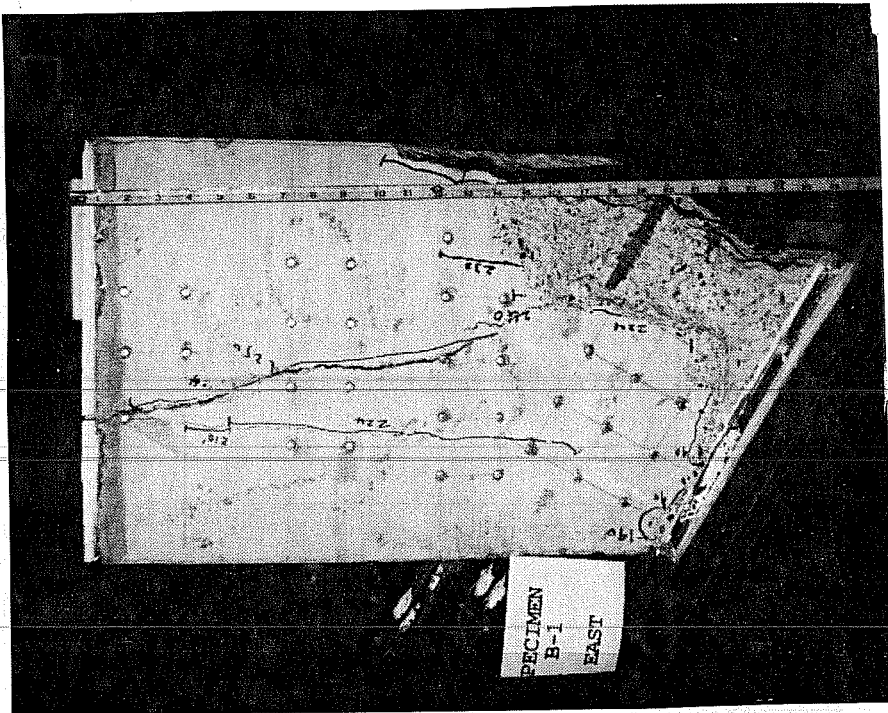
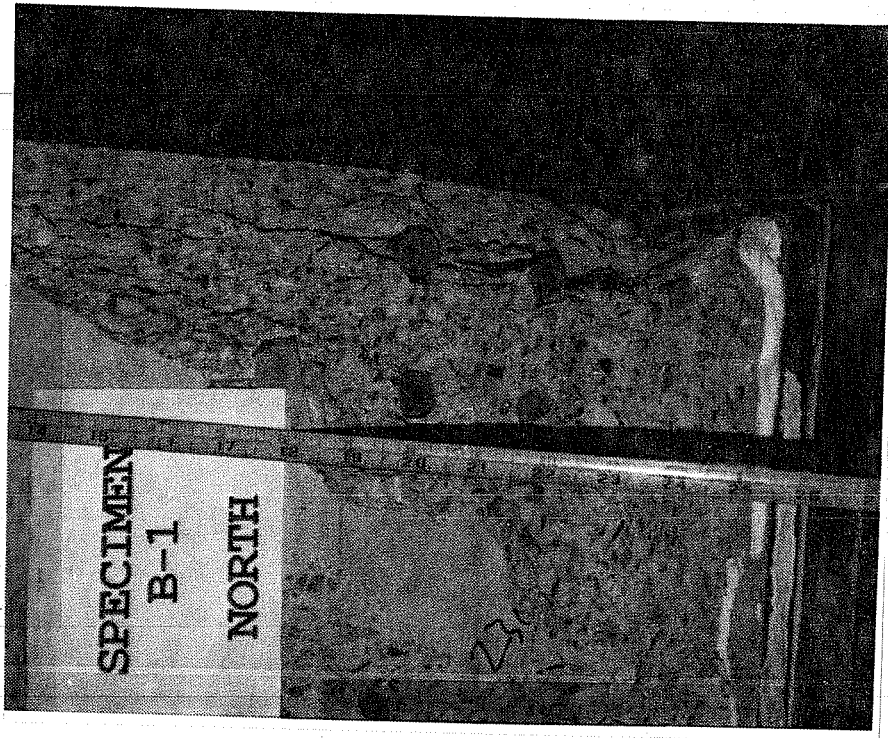


Fig. 4.6 Specimen B1 Crack Pattern

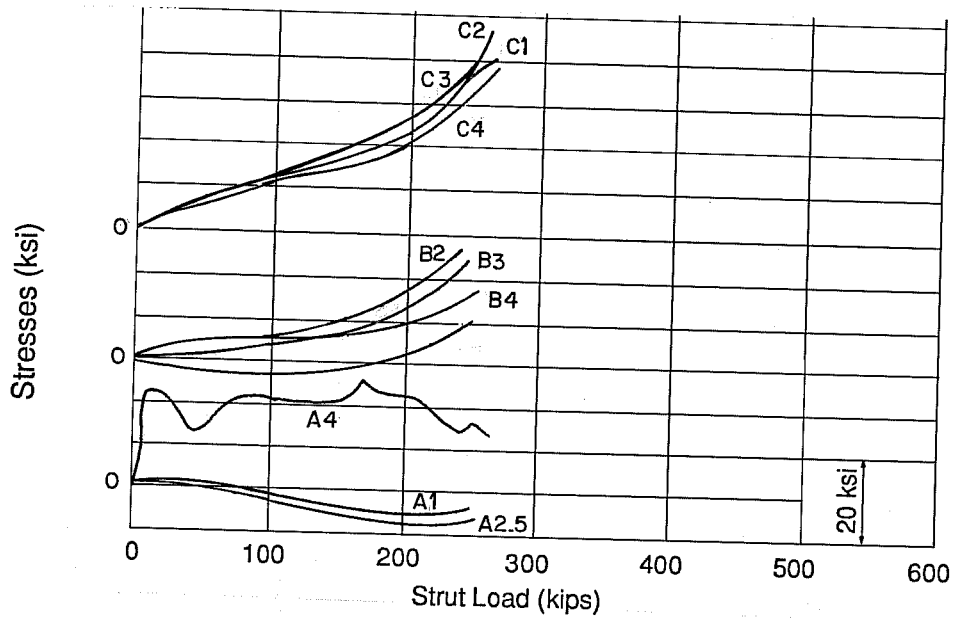


(a) East Face

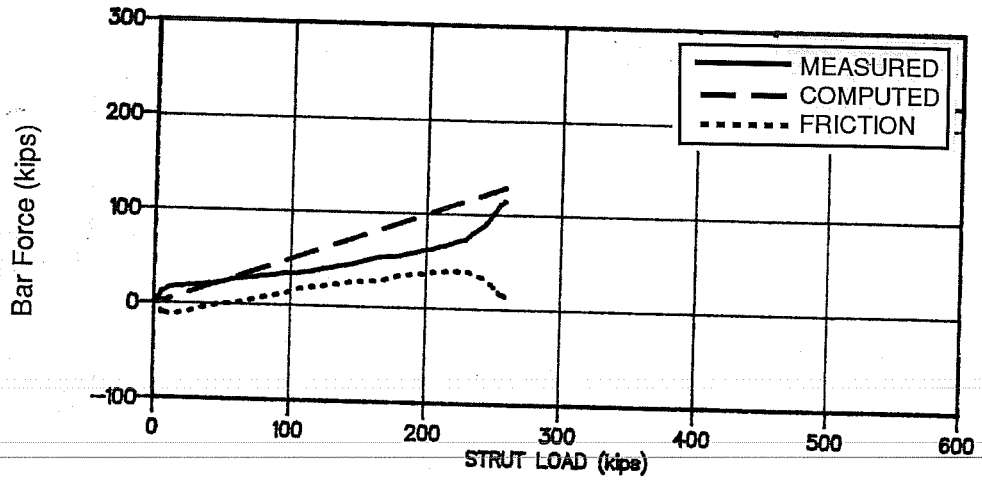


(b) West face

Fig 4.7 Specimen B1 after Failure



(a) Reinforcing Bar Stresses



(b) Reinforcing Bar Total Force

Fig. 4.8 Reinforcing Bar Stresses and Total Force (Specimen B1)

yielded. The measured total force in the bars was 18% less than the computed value (Fig.4.8b).

The distribution of the compressive concrete strain showed no clear pattern (Fig.4.9). The distribution of concrete tensile strains followed the observed crack pattern.

Specimen A2. In specimen A2 a reduced bearing area was used and transverse reinforcement was placed around the longitudinal bars.

The specimen failed in compression at a load of 240 kips. The first crack appeared at a load of 140 kips at the top loading surface. Figure 4.10 shows the crack pattern. At failure, a tensile crack appeared on the north face of the specimen (Fig 4.11).

The distribution on stresses in the bars was quite uniform (Fig.4.12a). The computed force acting on the bars was close to the measured value (Fig.4.12b).

The surface compressive strain was higher along the south edge (Fig.4.13). The very low values obtained along line CS4 may indicate that the load changed direction at that location. The highest concrete tensile strains were measured along a line where the major crack developed.

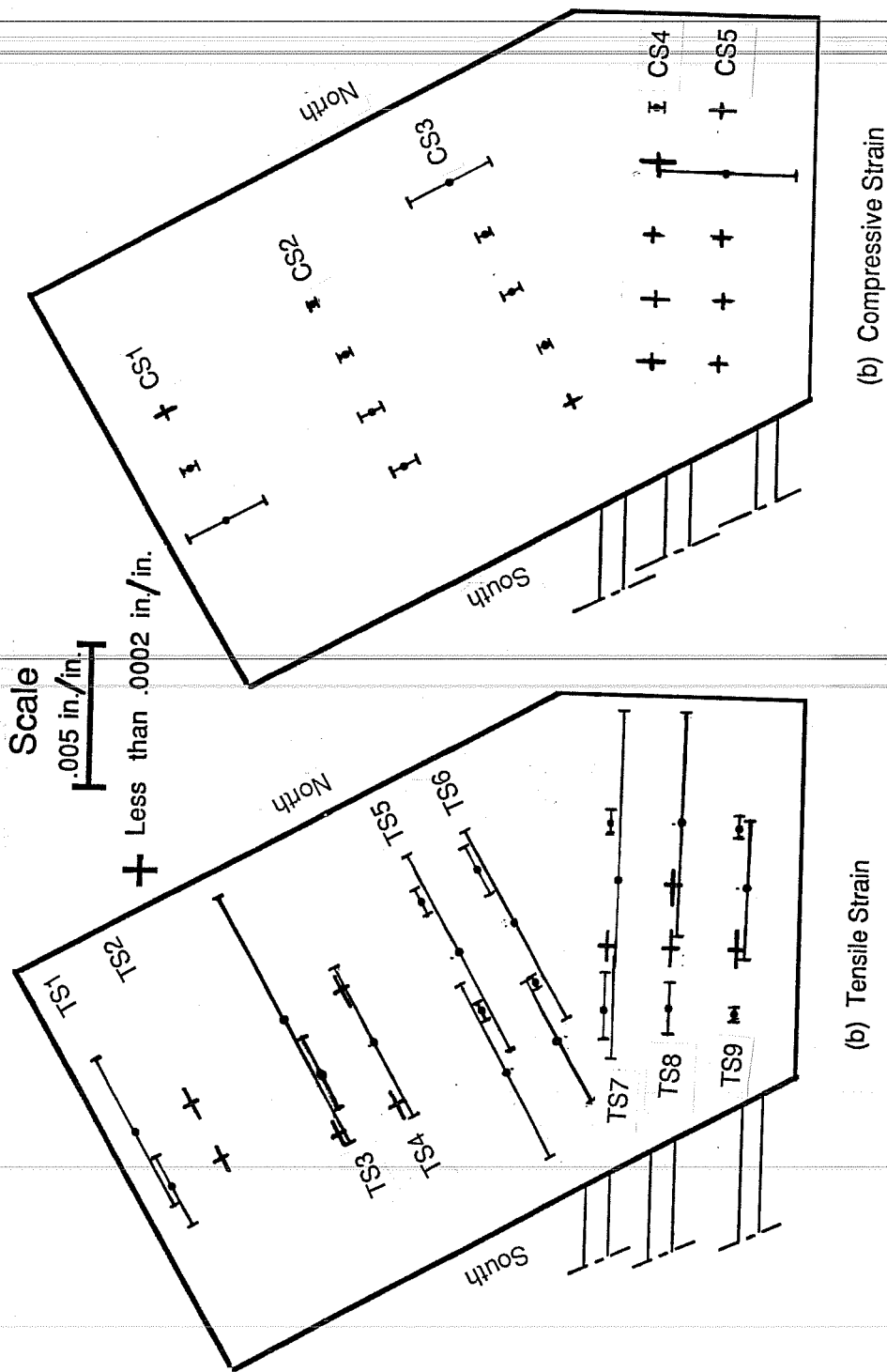


Fig. 4.9 Specimen B1 Surface Strain (Not Principal)

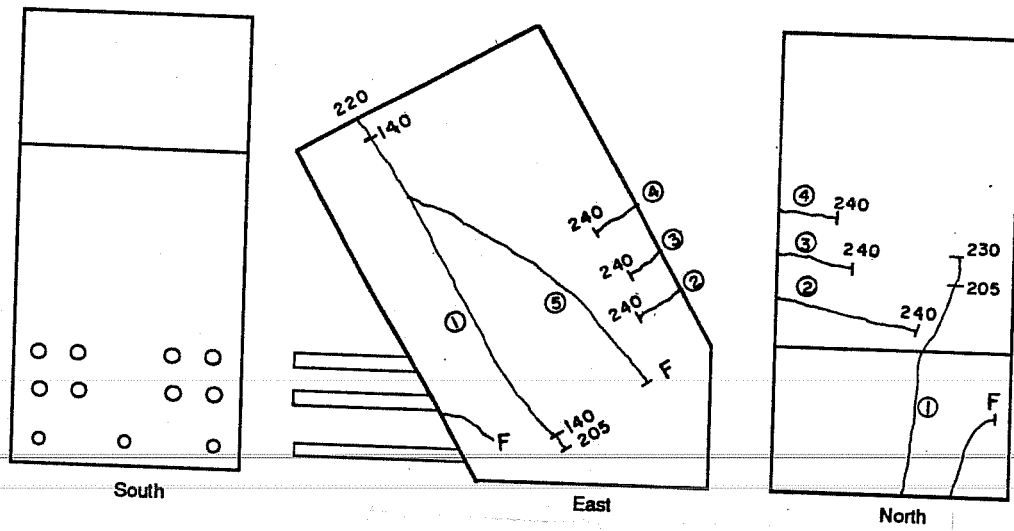
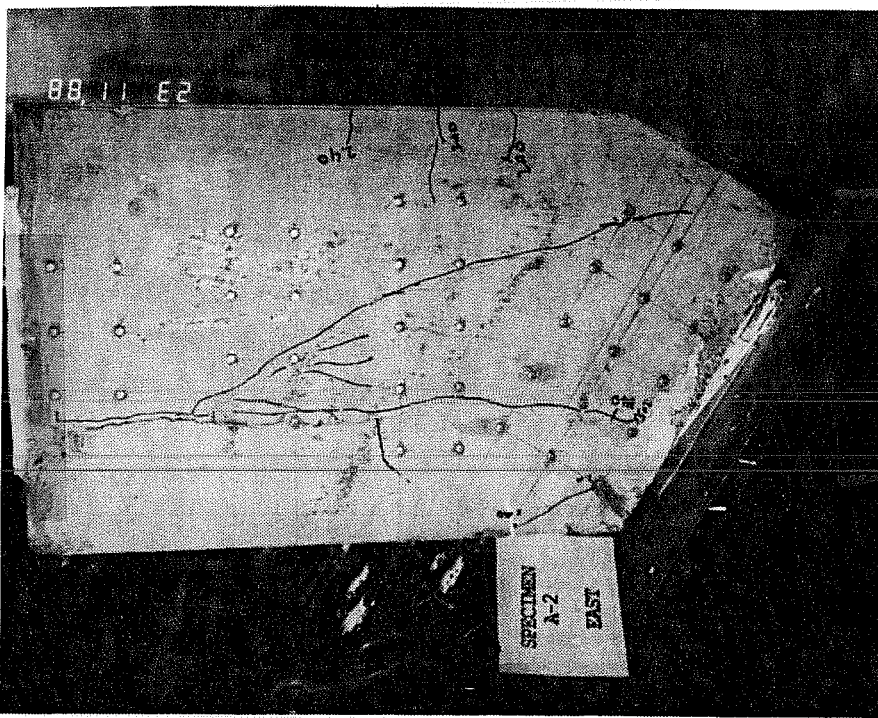
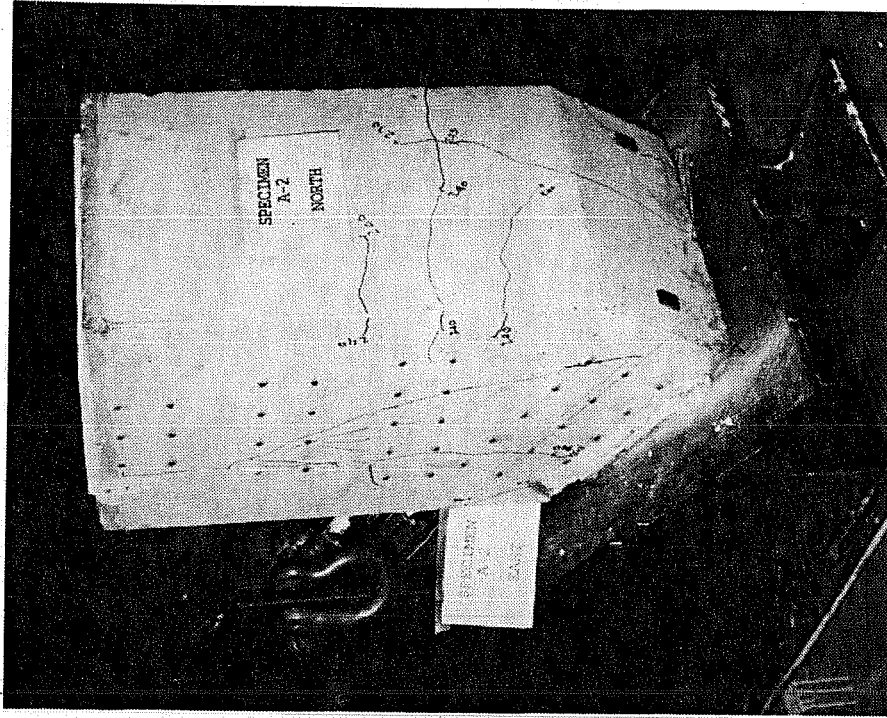


Fig. 4.10 Specimen A2 Crack Pattern

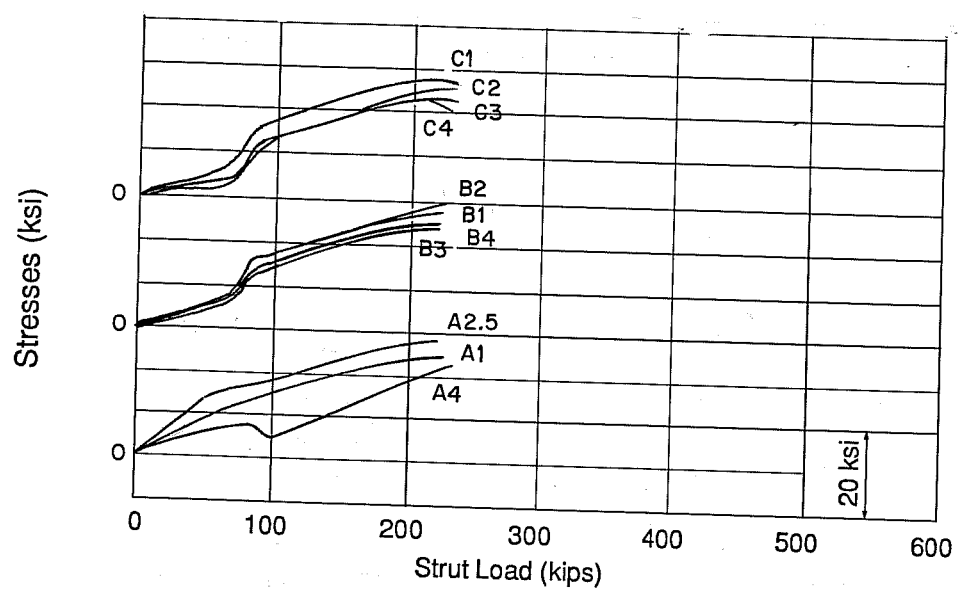


(a) East Face

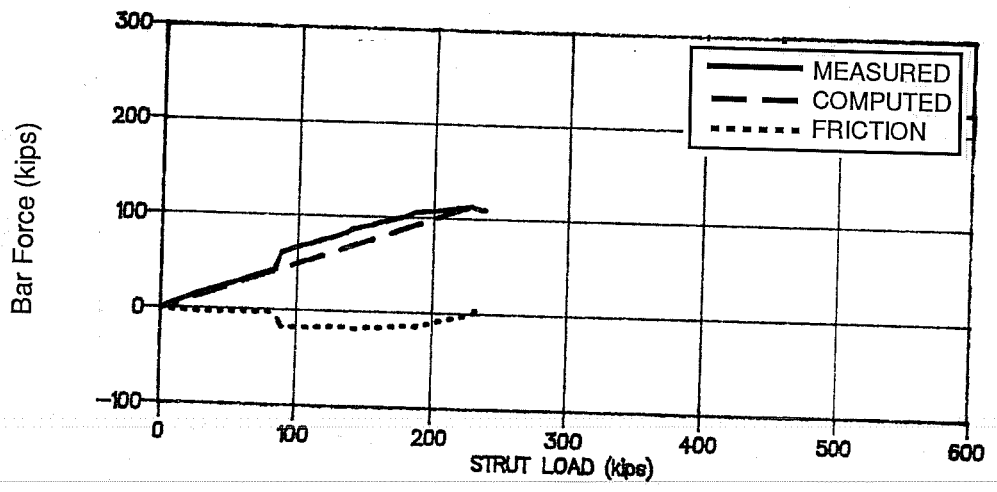


(b) North face

Fig 4.11 Specimen A2 after Failure



(a) Reinforcing Bar Stresses



(b) Reinforcing Bar Total Force

Fig. 4.12 Reinforcing Bar Stresses and Total Force (Specimen A2)

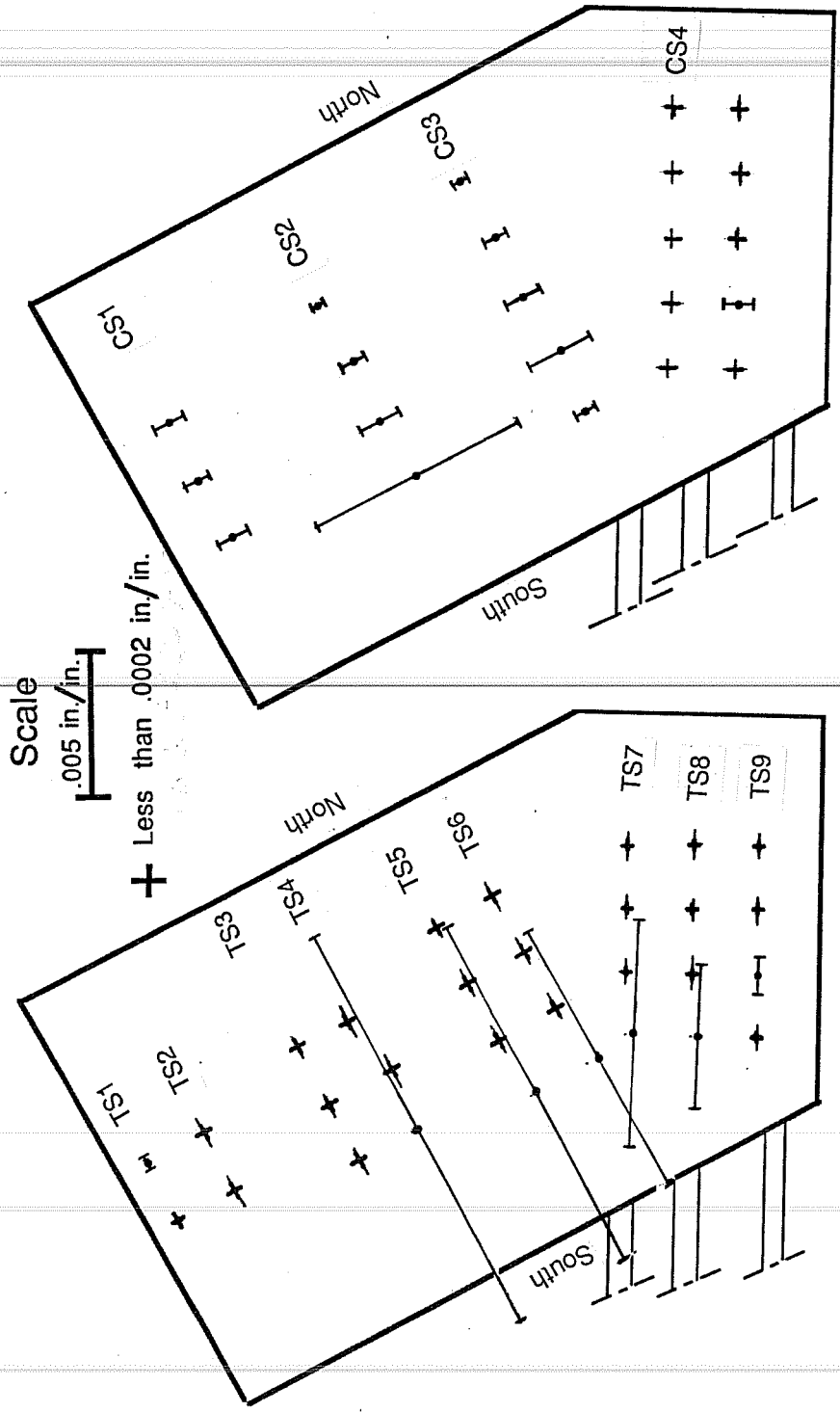


Fig. 4.13 Specimen A2 Surface Strain (Not Principal)

Specimen B2. Part of Series I, this specimen was tested to study the effect of reduced bearing area on the strength of unconfined concrete compressive strut.

The specimen failed at a load of 240 kips. The first crack, which developed at a load of 210 kips, started from the top part of the specimen at one edge of the loading plate (Fig.4.14). At failure that crack opened widely and ran through the specimen (Fig.4.15).

The bar forces were carried mainly by layer A (bottom layer). The other layers had either a low tensile or a compressive force. The stresses in layer A increased in a linear way at a high rate (Fig.4.16a). The average losses in the bar force was 30% (Fig.4.16b).

The principal compressive strains show that the load converged to the center of the support and spread in a bottle shape away from the support (Fig.4.17).

Specimen A1-R. Specimen A1-R was a replicate of specimen A1. However the thickness of the top loading plate was increased from 1 to 2 in to avoid uneven stress distribution on the loaded surface.

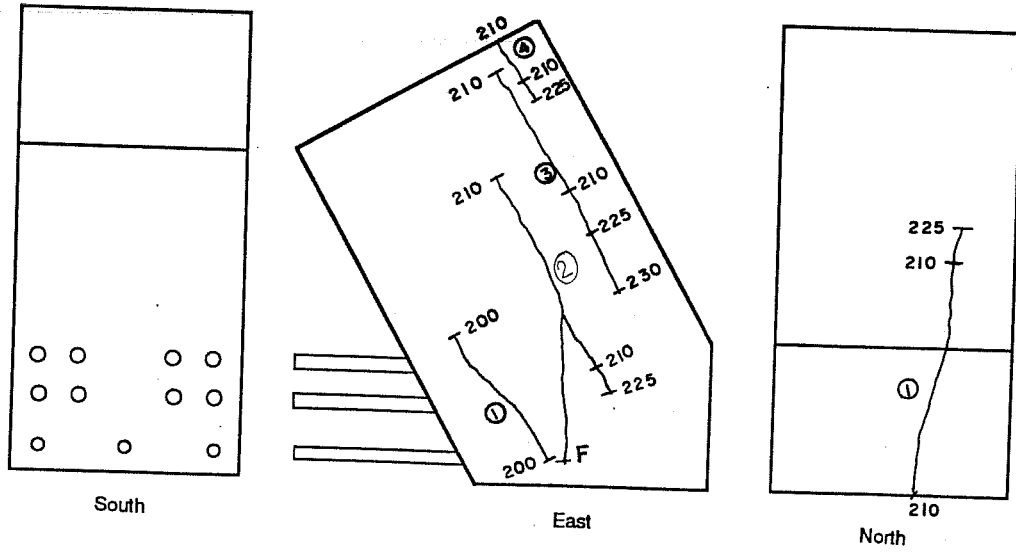
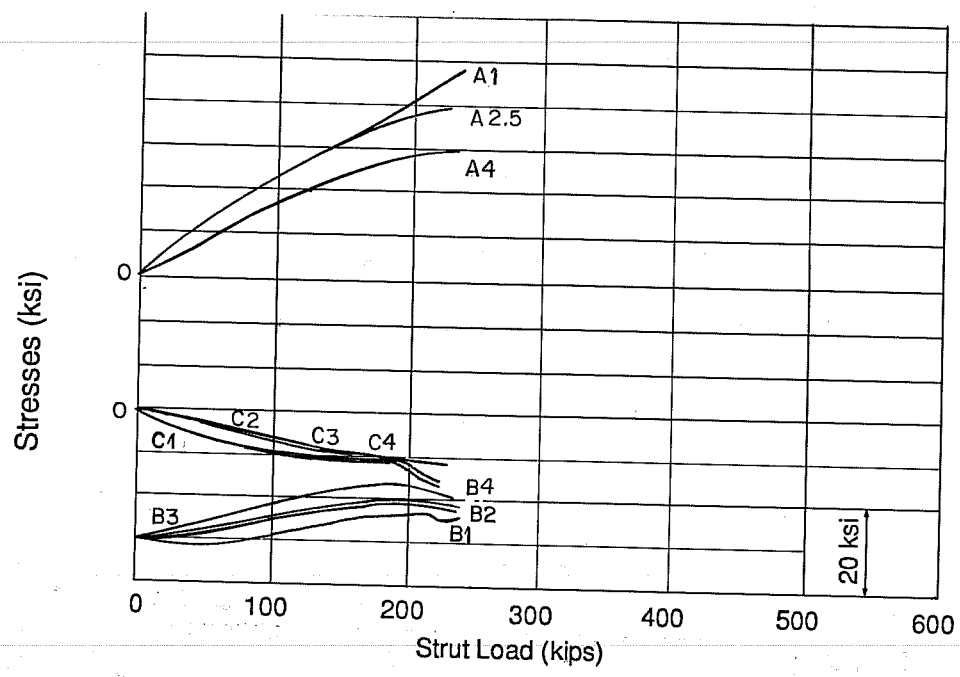
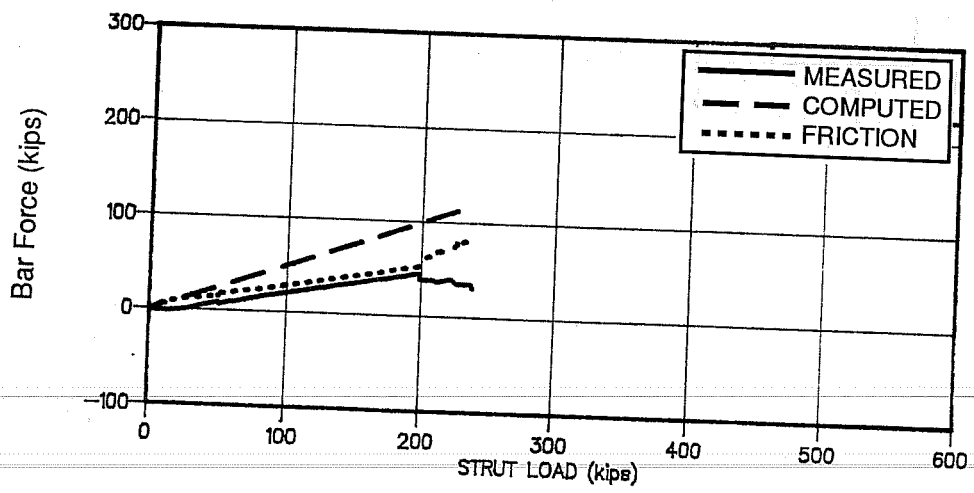


Fig. 4.14 Specimen B2 Crack Pattern



(a) Reinforcing Bar Stresses



(b) Reinforcing Bar Total Force

Fig. 4.16 Reinforcing Bar Stresses and Total Force (Specimen B2)

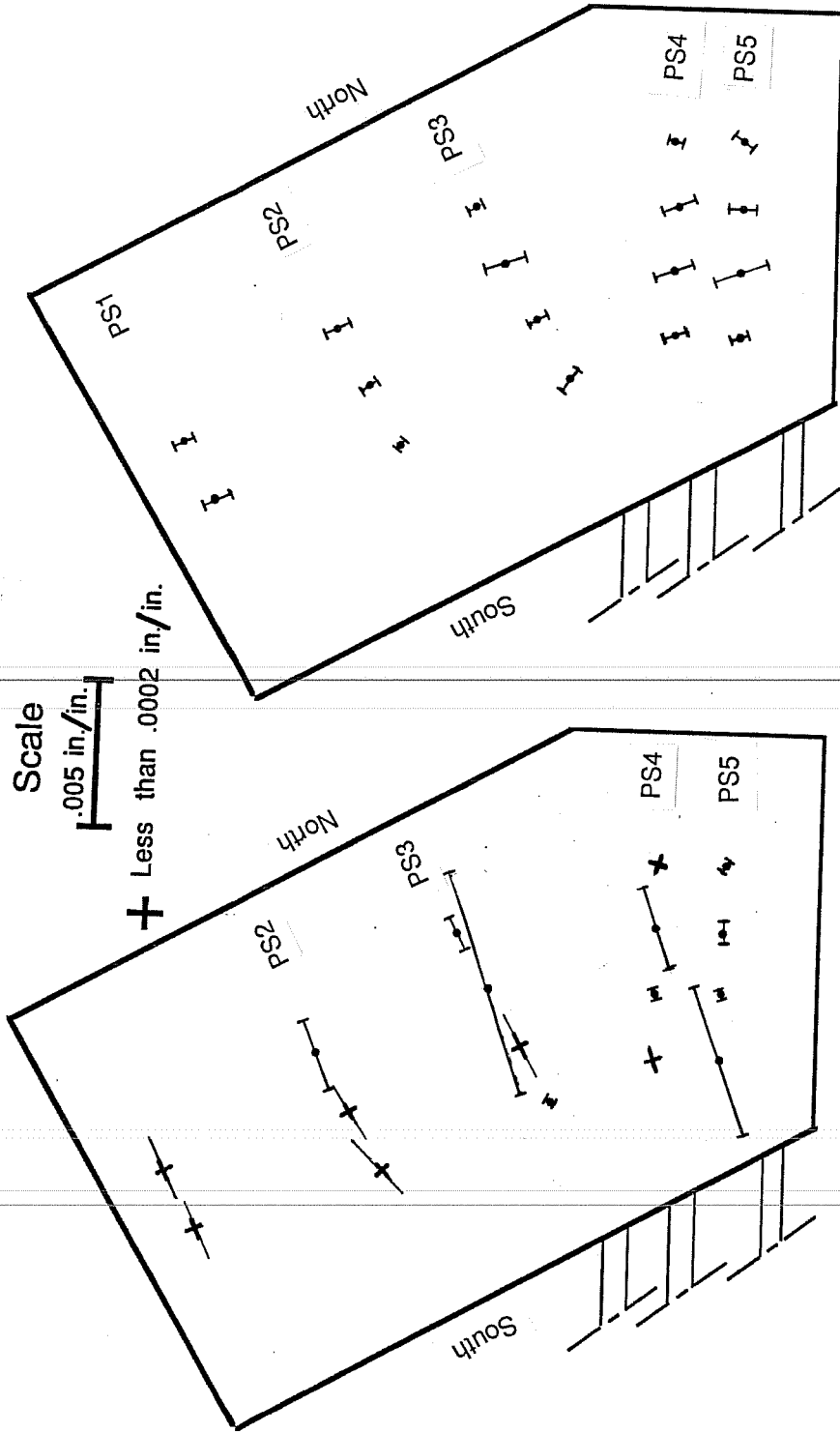


Fig. 4.17 Specimen B2 Principal Surface Strain

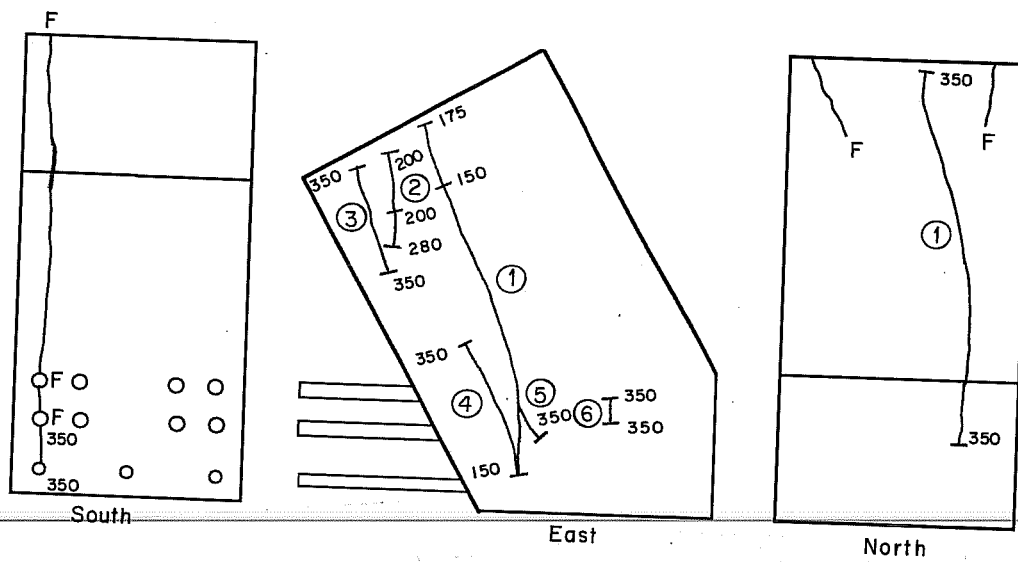


Fig. 4.18 Specimen A1-R Crack Pattern

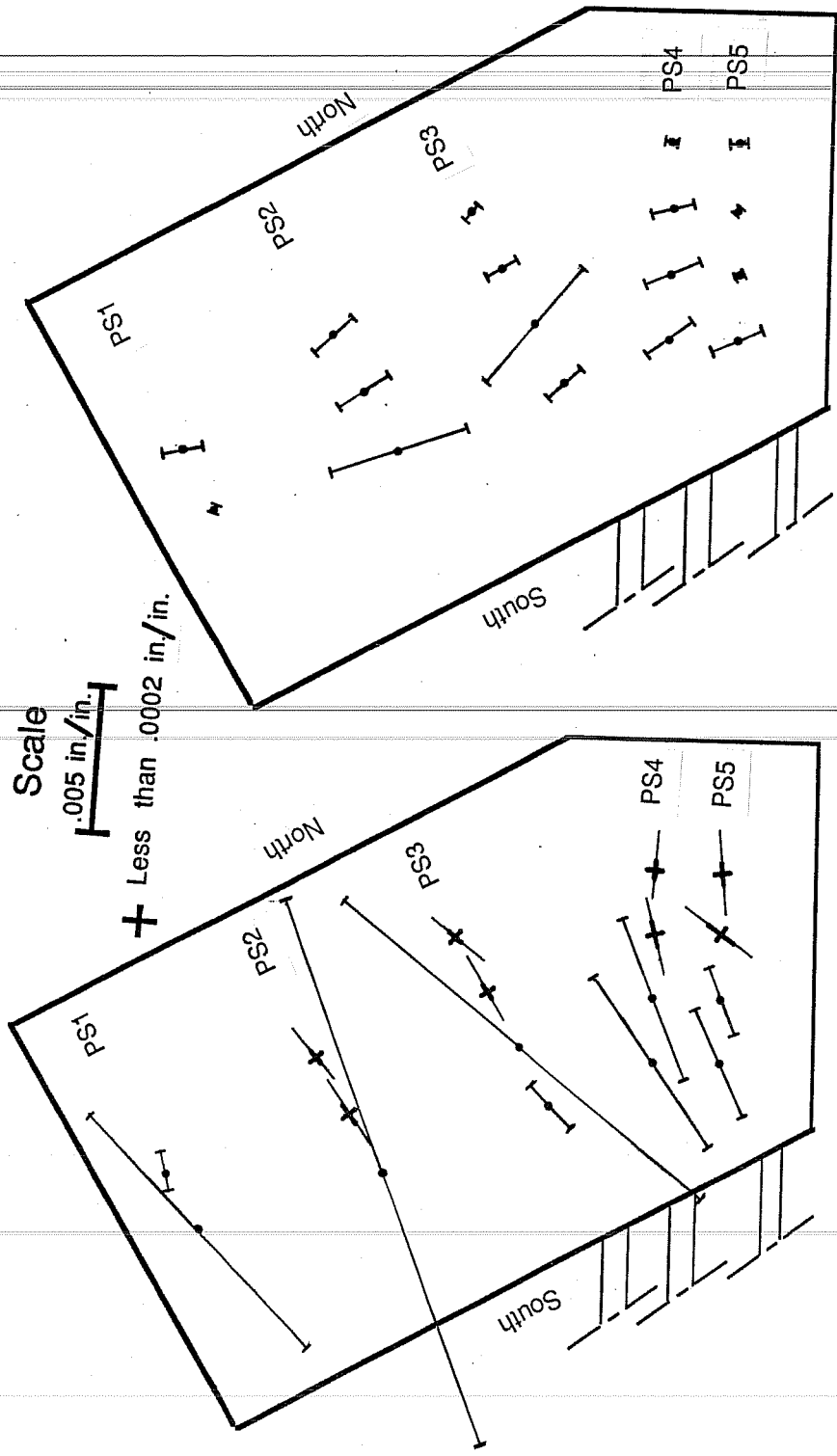
The first crack appeared at a load of 150 kips (Fig.4.18) and was due to the compressive force on the strut. The specimen failed at a load of 350 kips. A large crack that ran from top to bottom of the specimen (Fig.4.19a) shows that the teflon was working well and no restraint was provided by the loading plate.

Spalling of the cover concrete and the appearance of the transverse reinforcement at failure (Fig.4.19b) shows that the hoops increased the specimen capacity by preventing an anchorage failure.

The stresses on the longitudinal bars were unevenly distributed among the different layers. The rate of stress increase and the stresses were higher for layer C (upper layer). Layer A (bottom layer) had low stresses (Fig.4.20a). The total force acting on the bars was about 15% less than computed values. Figure 4.20b shows the load distribution on the longitudinal bars.

The principal surface compressive strain are shown in Figure 4.21. High strains were measured along the crack location. The strain values show that the crack were restrained in the part of the specimen which had transverse reinforcement.

Specimen A1-2. Specimen A1-2 had the same reinforcement configuration as specimen A1 but was cast with higher strength concrete.



(a) Tensile Strain

(b) Compressive Strain

Fig. 4.21 Specimen A1-R Principal Surface Strain

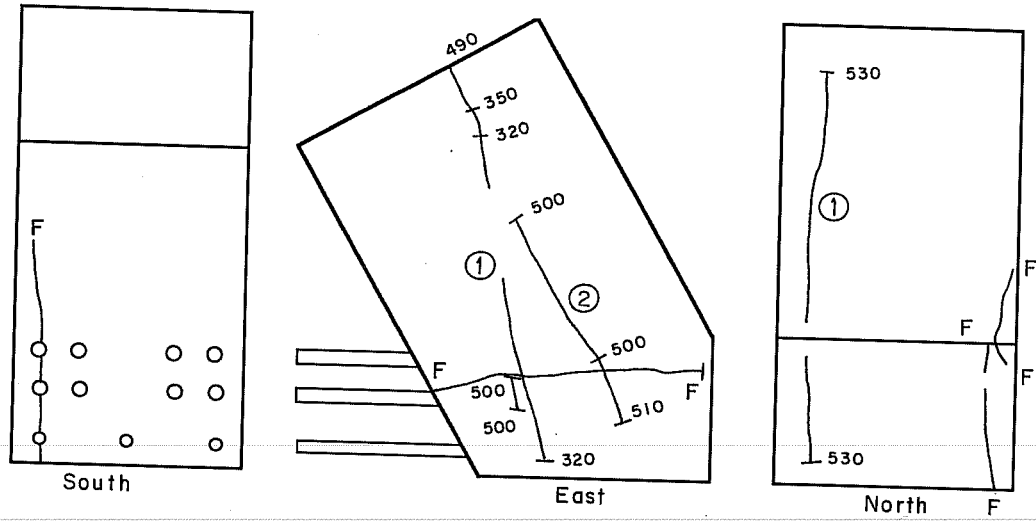


Fig. 4.22 Specimen A1-2 Crack Pattern

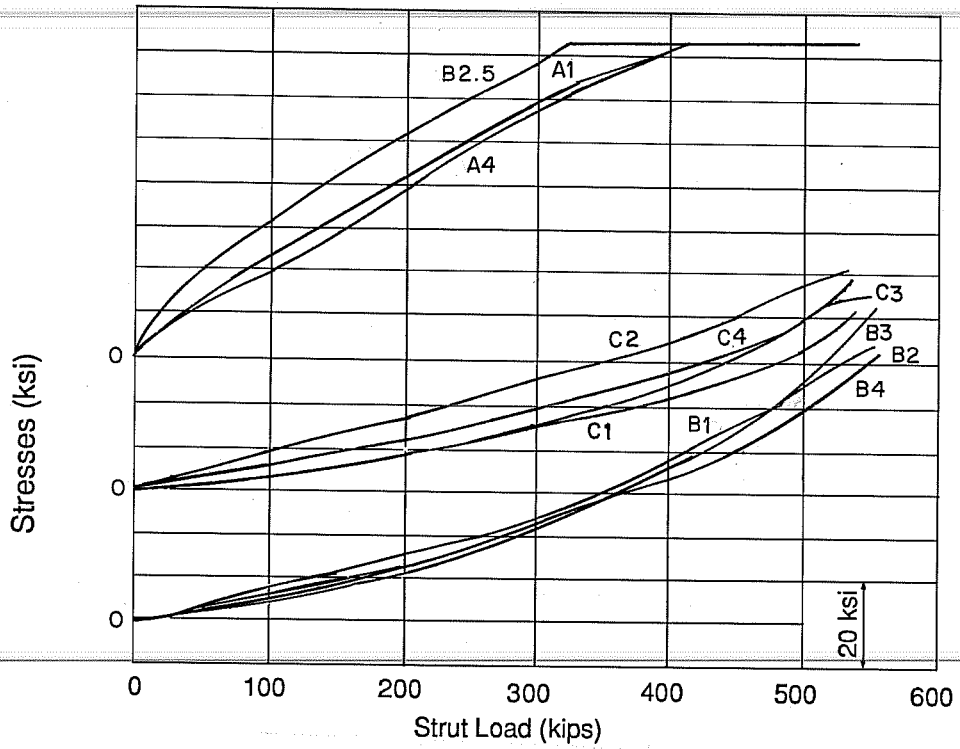
The specimen failed in anchorage at a load of 540 kips by splitting of the side cover (Fig.4.23). The first crack appeared at a load of 320 kips and started from the support surface. Figure 4.22 shows the crack pattern.

The load in the bars increased almost linearly for each layer. The bottom layer reached the highest stresses. All the bars of the bottom layer yielded at a load of 400 kips (Fig.4.24a). The frictional losses were around 7% of applied load Figure 4.24b shows the bar force.

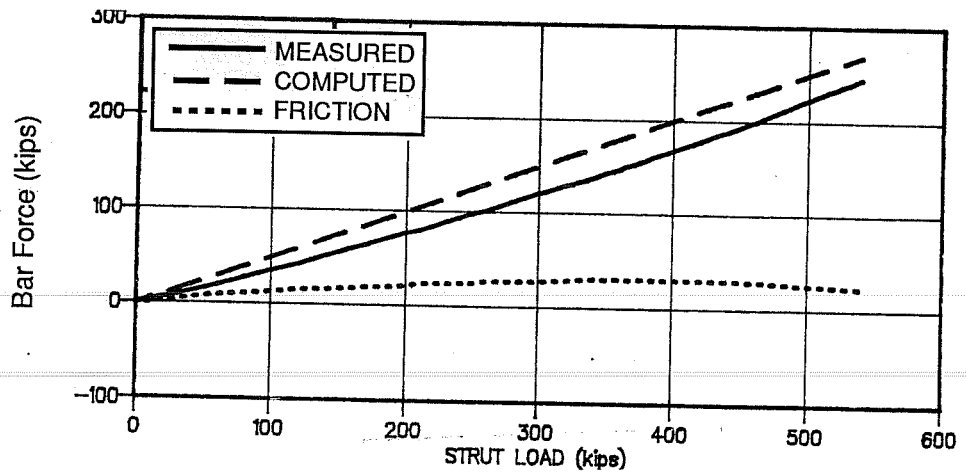
The surface principal strains indicate that the load was concentrated in the center of the specimen away from that part of the specimen which had transverse reinforcement (Fig.4.25). The compressive force appear to shift slightly away from the center towards the south face near the support surface.

Specimen C1. Specimen C1 was tested to evaluate the anchorage along straight bars.

The specimen failed in anchorage at a load of 450 kips by splitting of the side (Fig.4.27). The first crack appeared at a load of 300 kips and made an angle of 65° with the reinforcement (Fig.4.26).

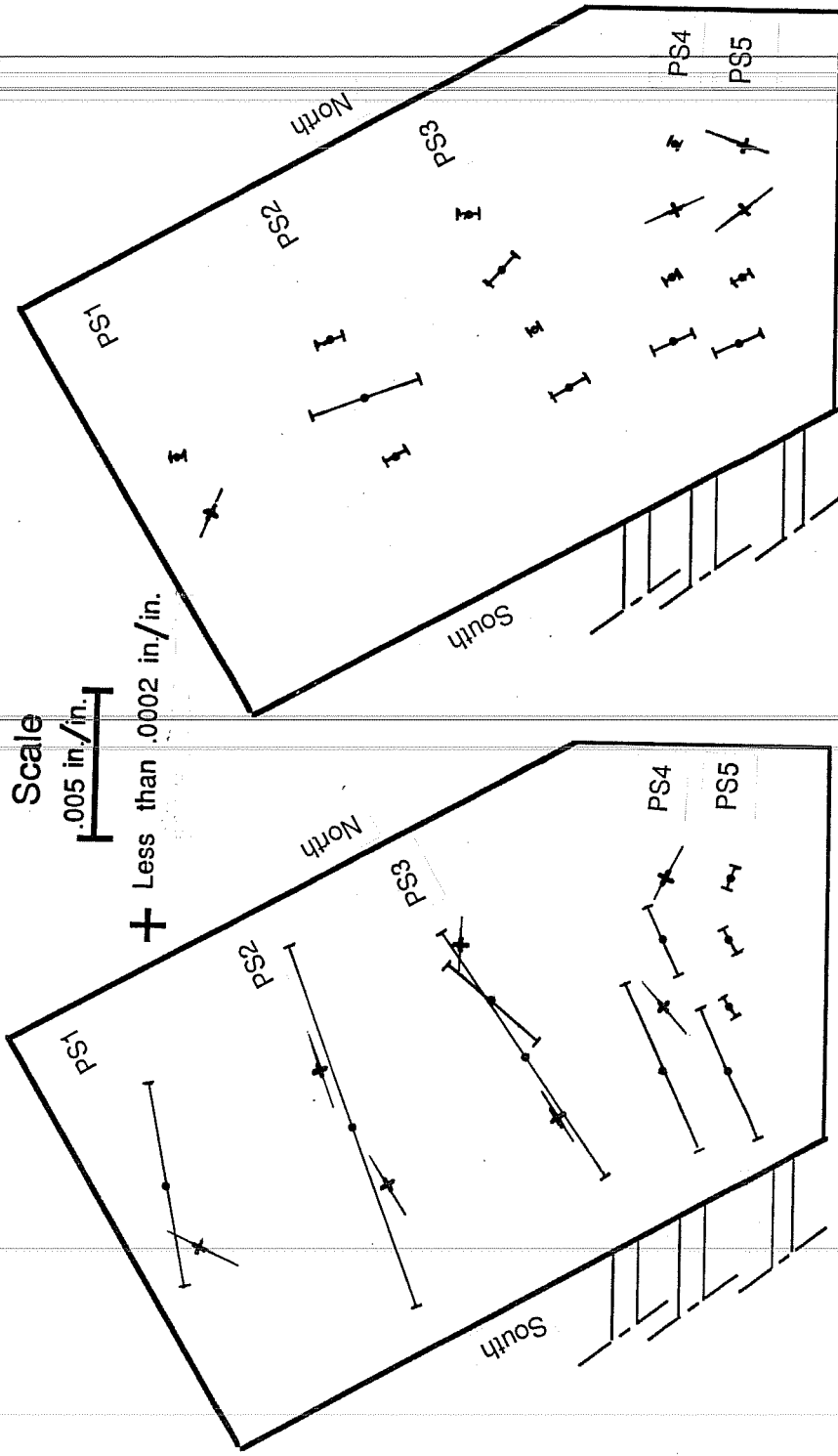


(a) Reinforcing Bar Stresses



(b) Reinforcing Bar Total Force

Fig. 4.24 Reinforcing Bar Stresses and Total Force (Specimen A1-2)



(a) Tensile Strain

(b) Compressive Strain

Fig. 4.25 Specimen A1-2 Principal Surface Strain

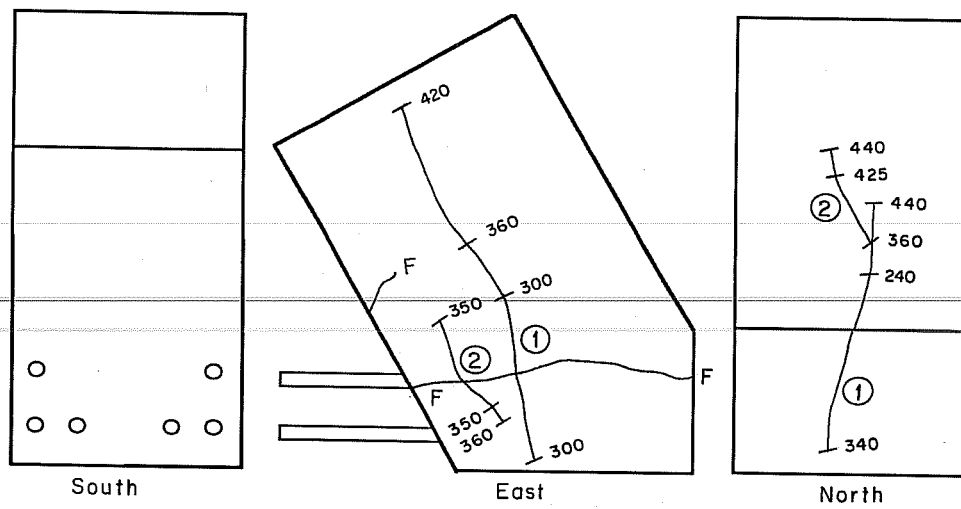
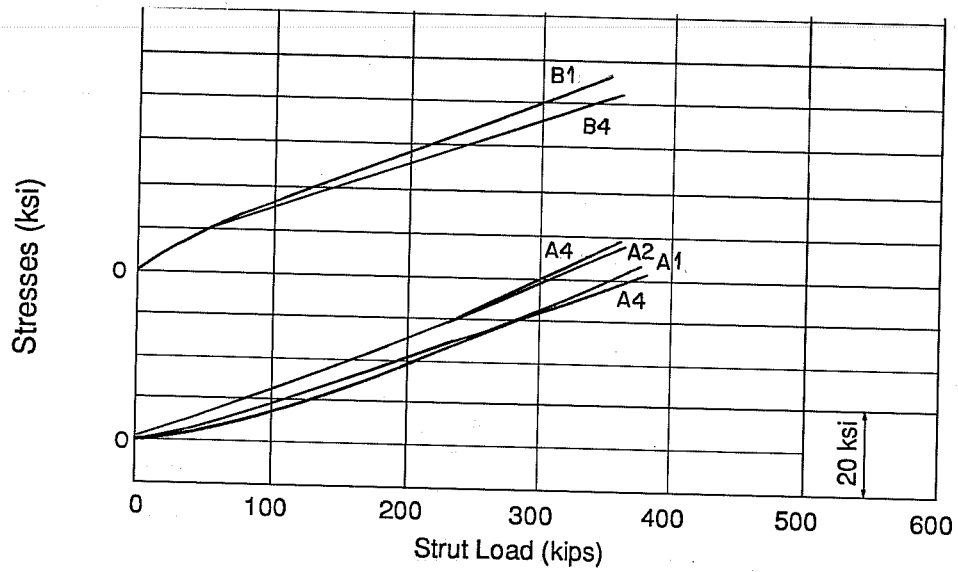
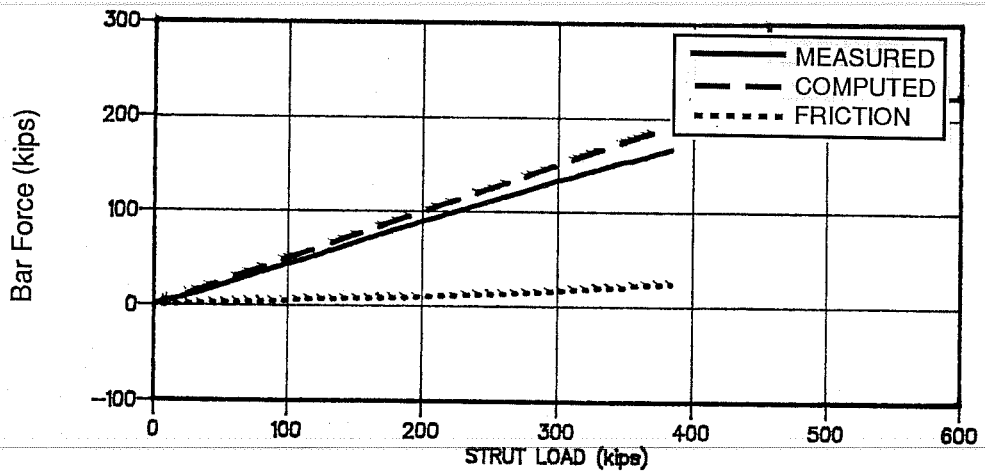


Fig. 4.26 Specimen C1 Crack Pattern



(a) Reinforcing Bar Stresses



(b) Reinforcing Bar Total Force

Fig. 4.28 Reinforcing Bar Stresses and Total Force (Specimen C1)

The load was evenly distributed among the bars. The losses were low (average of 6%). Figure 4.28 shows the load distribution on the bars.

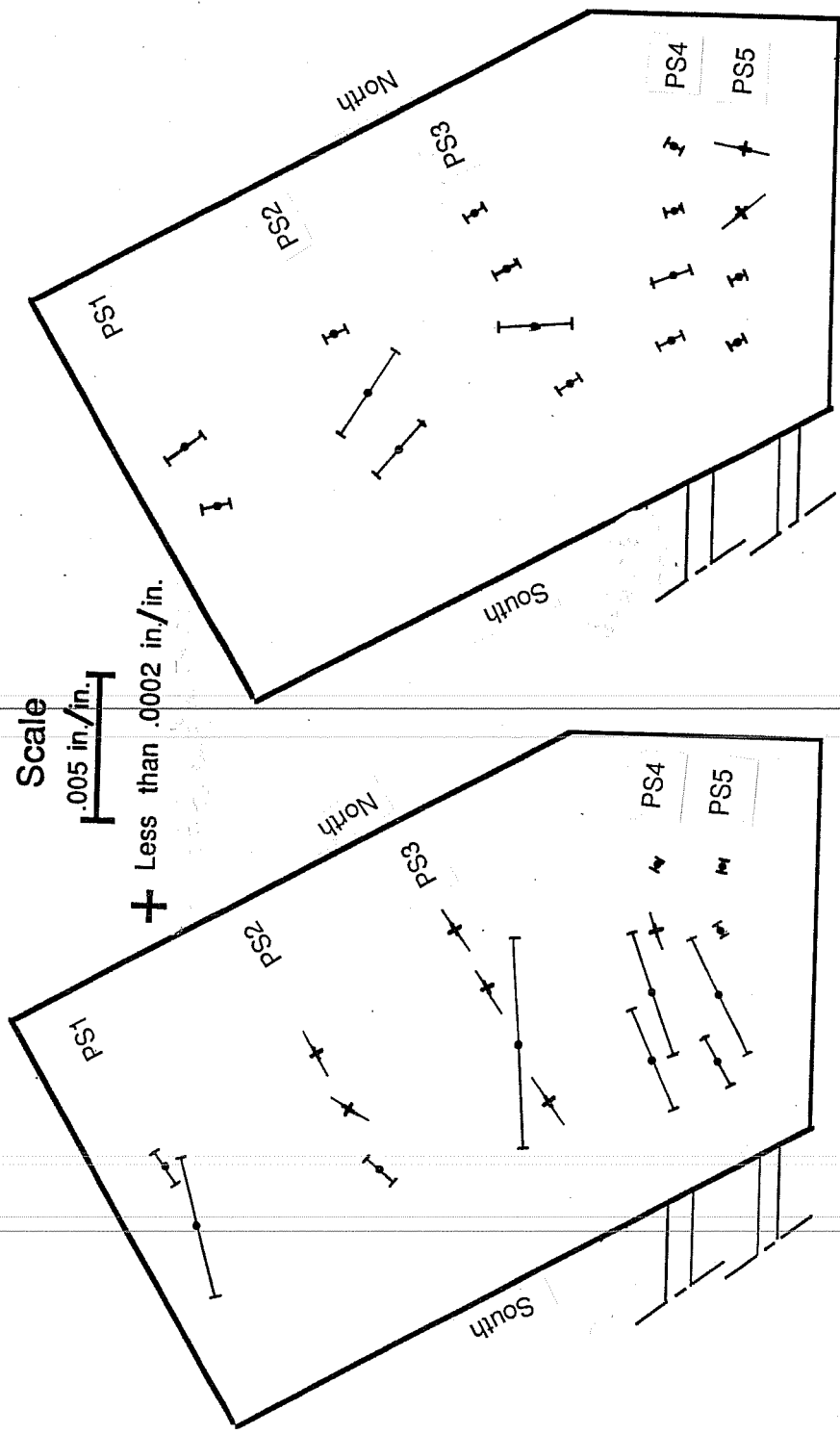
The surface strain (Fig.4.29) shows that the line of action of the compressive force in the concrete is located toward the south edge. The load converges to the center at the top support.

Specimen C2. Specimen C2 was tested to investigate the effect of hooks on the development length of bars.

The first crack was located at 2.5 in. from the south face and developed at a load of 310 kips. A major crack appeared in the middle of the face at a load of 340 kips and made an angle of 65° with the longitudinal reinforcement. Figure 4.30 shows the crack pattern. The specimen failed in anchorage at a load of 415 kips by splitting of the side cover (Fig.4.31).

During transportation, the specimen fell and had some cracks on the West face that were repaired using epoxy. The epoxy probably resulted in cracks not appearing at early stages on the West face of the specimen.

The bar stresses increased linearly except for the bar A3. It showed a decrease in force at an applied load of 90 kips. This may be due to a loss in bond capacity. The friction losses in the



(a) Tensile Strain

(b) Compressive Strain

Fig. 4.29 Specimen C1 Principal Surface Strain

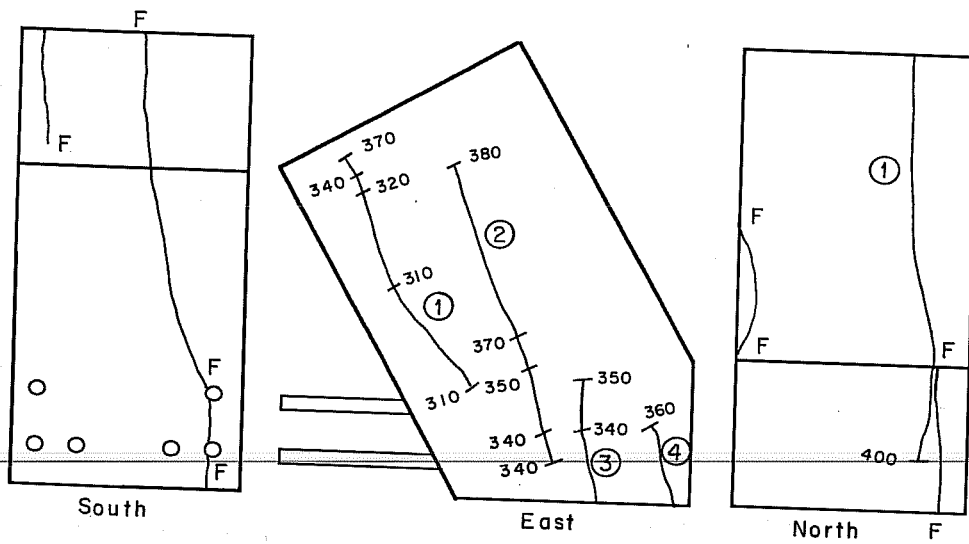
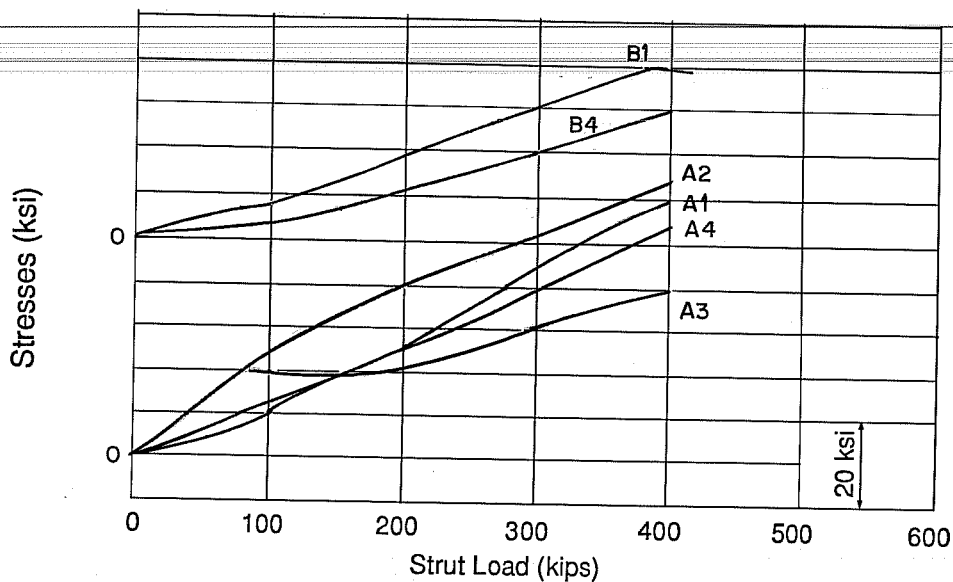
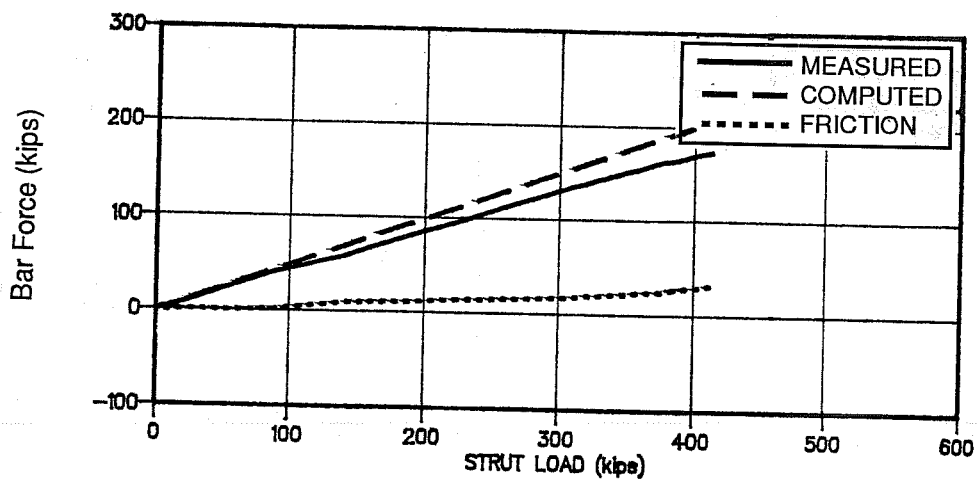


Fig. 4.30 Specimen C2 Crack Pattern



(a) Reinforcing Bar Stresses



(b) Reinforcing Bar Total Force

Fig. 4.32 Reinforcing Bar Stresses and Total Force (Specimen C2)

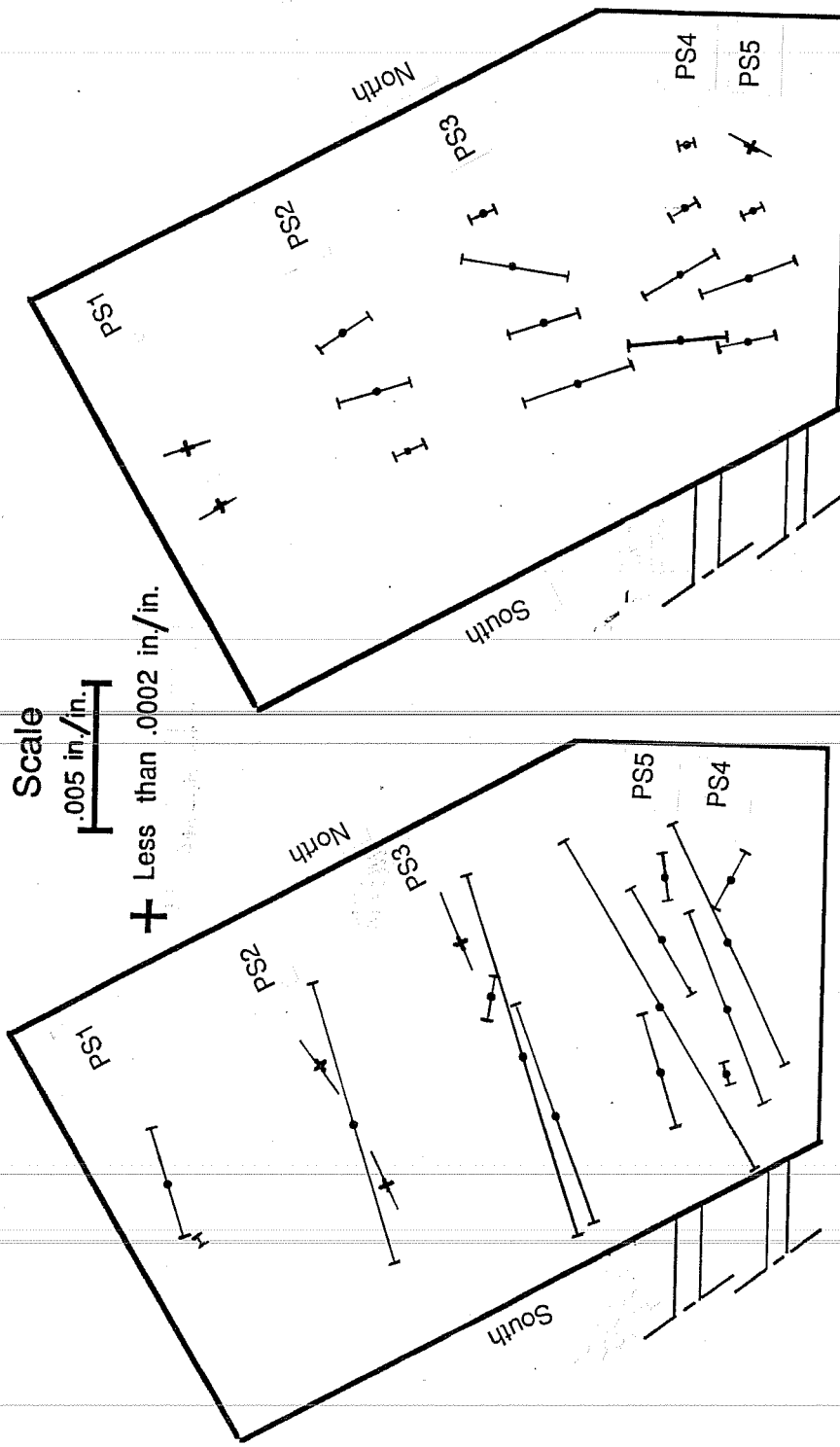


Fig. 4.33 Specimen C2 Principal Surface Strain

total force carried by the reinforcement were around 7%. Figure 4.32 shows the distribution of the load on the longitudinal bars.

Figure 4.33 shows the principal surface strain.

Specimen D1. Specimen D1 was tested to evaluate the effect of concrete cover on the development length of straight bars.

The first crack, due to the compressive force, appeared at a load of 300 kips. It started from the loading surface and was located mainly in the middle of the face. Figure 4.34 shows the crack pattern. The specimen failed at a load of 470 kips by splitting of the side cover (Fig.4.35).

Bars C4 and B3 carried less load. Bar B4 experienced a loss of load at a load of 340 kips which can be attributed to a loss in bond capacity. The losses were around 7%. Figure 4.36 shows the load distribution on the longitudinal bars.

The principal surface strain are shown in Figure 4.37.

Specimen D2. Specimen D2 was tested to evaluate the effect of cover and hooks on the development length of reinforcing bars.

Uneven bearing of the loading plate caused poor performance at early loading stages and cracks prematurely developed at a load of 200 kips. To improve the test conditions, the specimen was unloaded, and the bearing conditions of the plate were improved

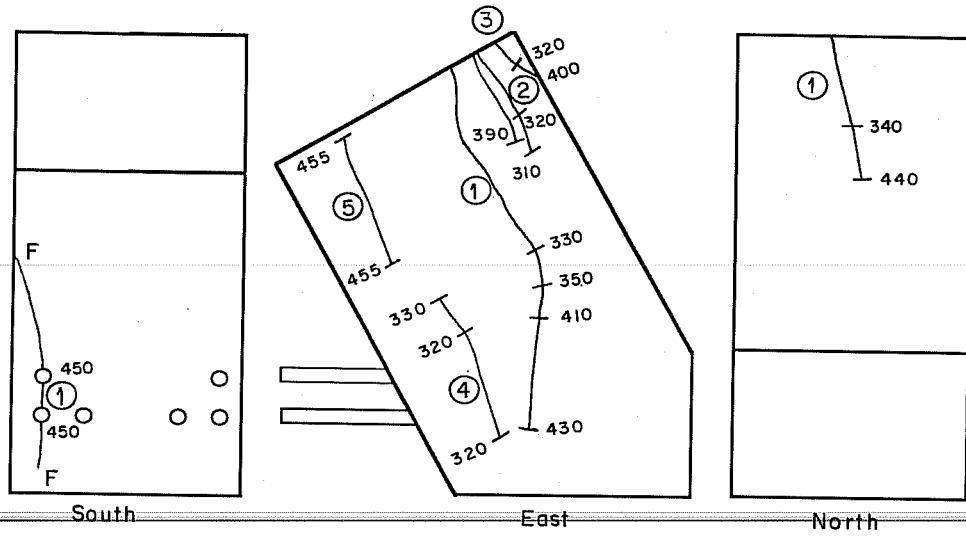


Fig. 4.34 Specimen D1 Crack Pattern

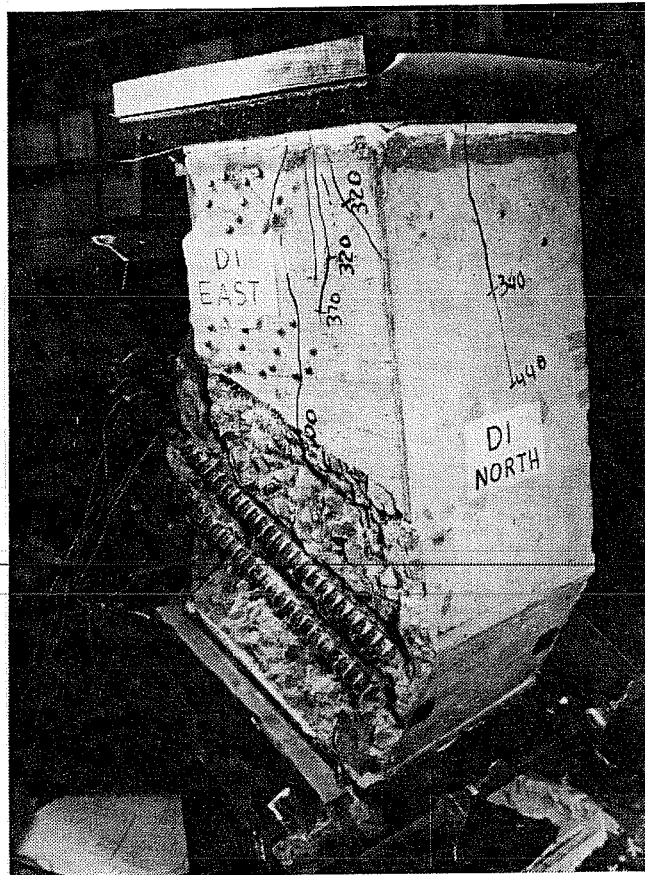
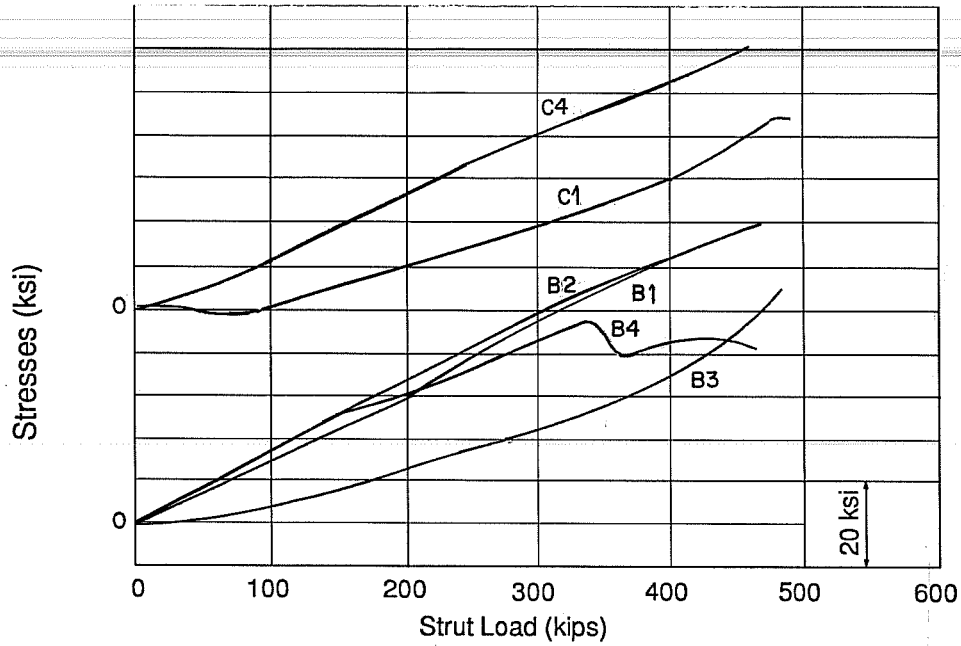
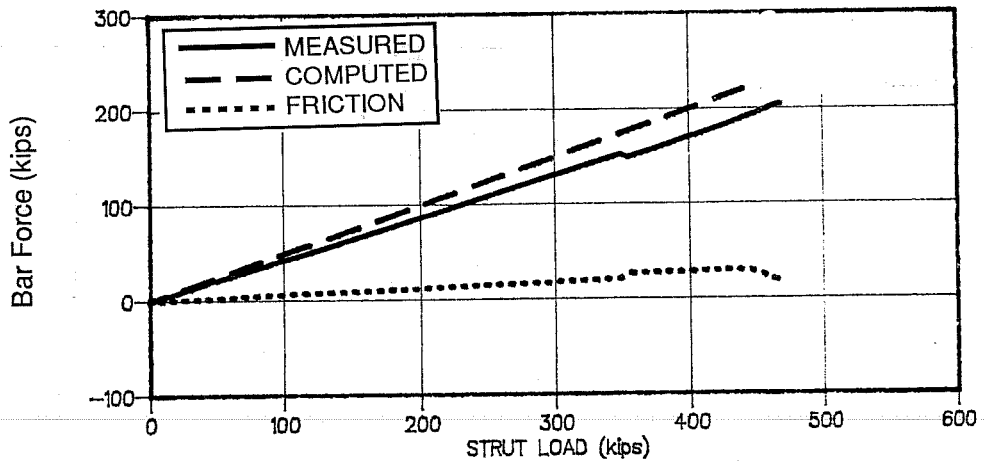


Fig 4.35 Specimen D1 after Failure



(a) Reinforcing Bar Stresses



(b) Reinforcing Bar Total Force

Fig. 4.36 Reinforcing Bar Stresses and Total Force (Specimen D1)

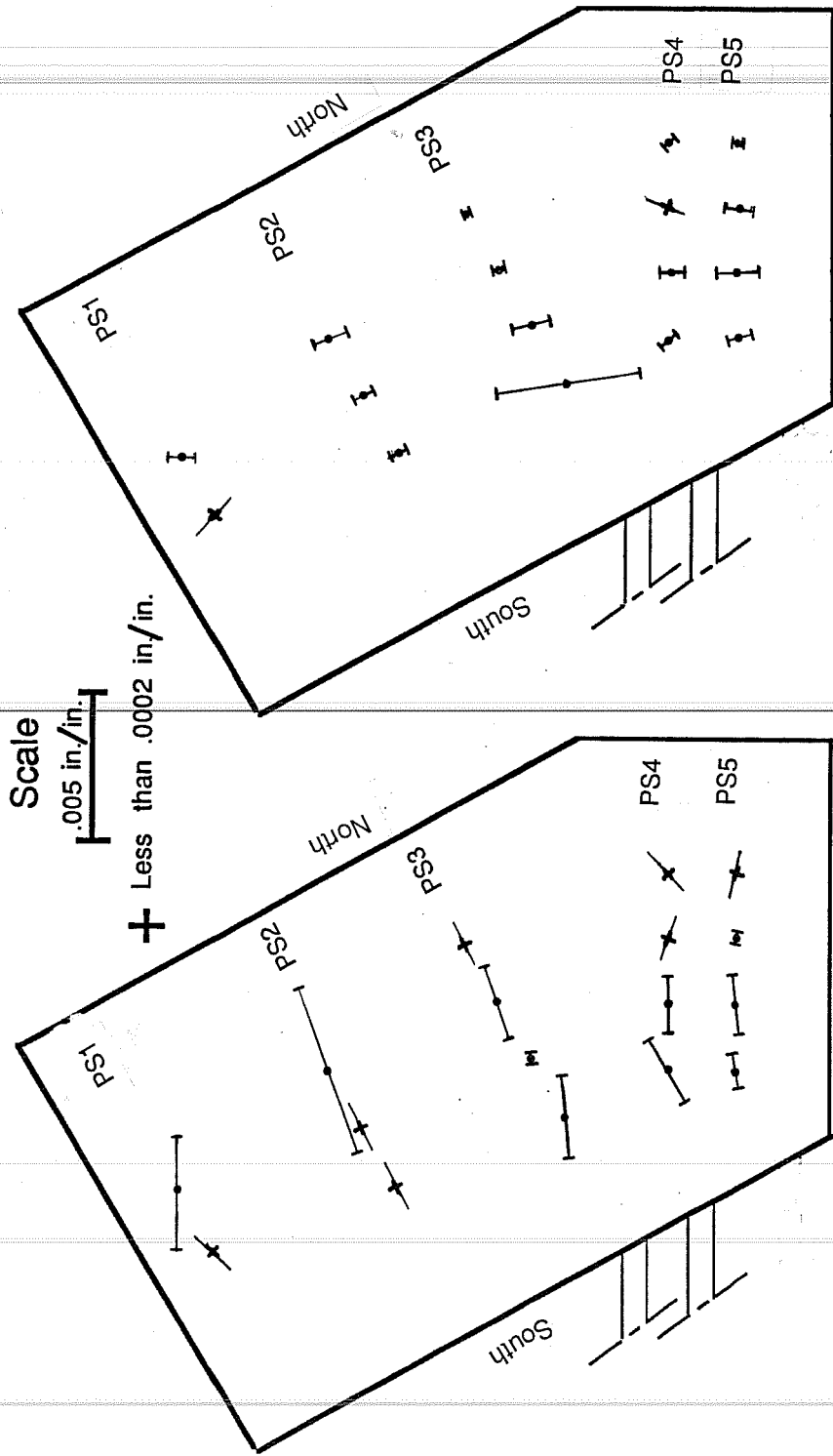


Fig. 4.37 Specimen D1 Principal Surface Strain

as described in chapter 3. The specimen was then reloaded without further problems.

Cracks appeared again at a load of 310 kips. The first crack went from top to bottom of the specimen and was located approximately in the middle of the side face. Other cracks appeared on the lower part of the specimen. Figure 4.38 shows the crack pattern.

The specimen failed at a load of 435 kips by splitting of the side cover (Fig.4.39). This splitting occurred on both faces. The failure was brittle and sudden.

The load in the bars was quite evenly distributed among the bars of the same layer. The stresses in the bars of layer B were twice as much as those of the layer C. The frictional losses were around 6%. Figure 4.40 shows the bar load.

The surface principal strain (Fig.4.41) shows that the stress trajectory has a bottle shape. The strain had, in general, the same average value along a given line.

4.3 Comparison of Experimental Results

Failure modes and failure loads are summarized in Table 4.1.

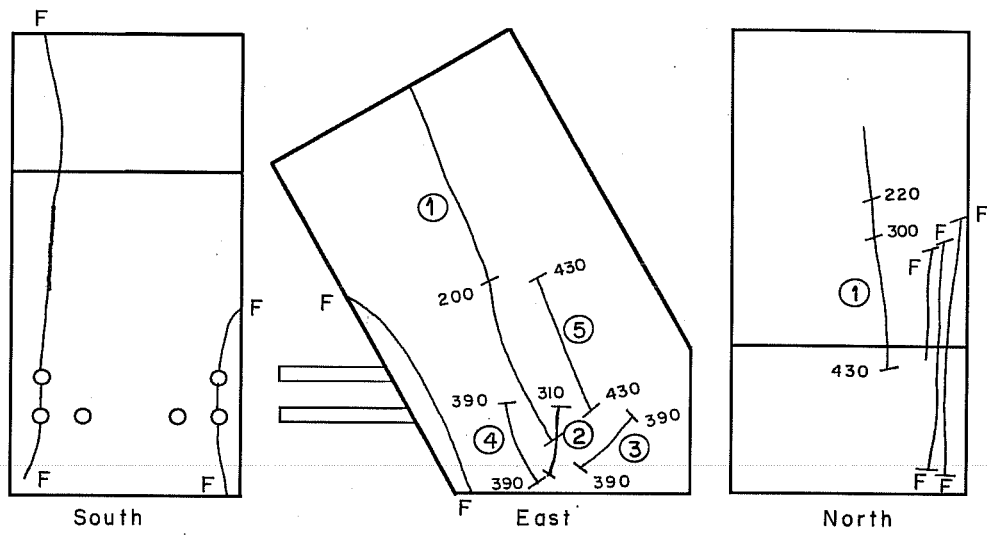
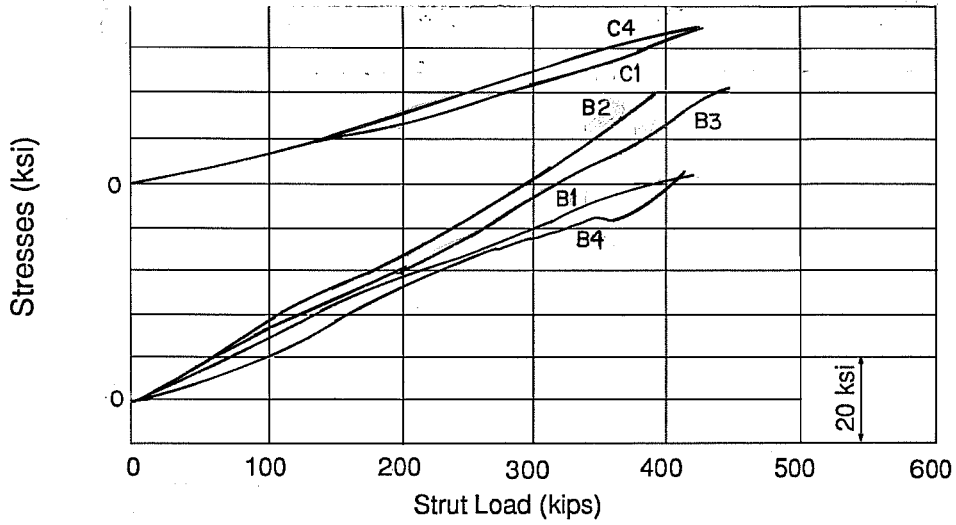
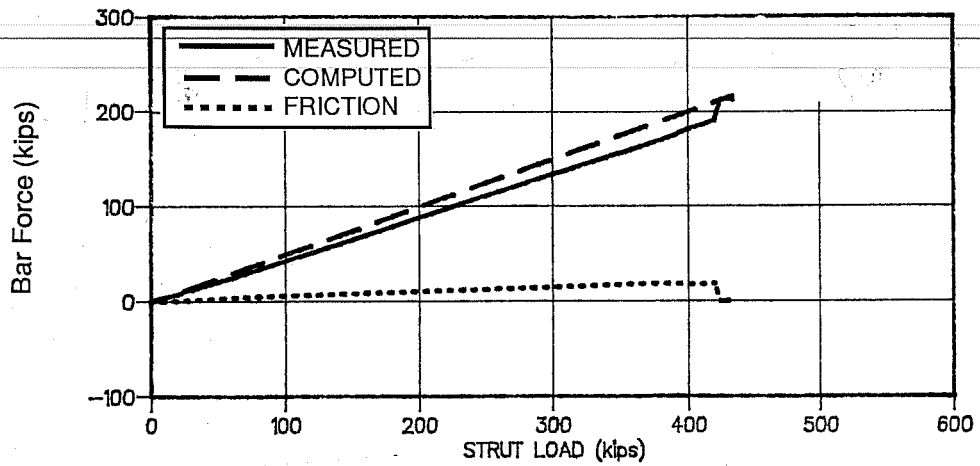


Fig. 4.38 Specimen D2 Crack Pattern



(a) Reinforcing Bar Stresses



(b) Reinforcing Bar Total Force

Fig. 4.40 Reinforcing Bar Stresses and Total Force (Specimen D2)

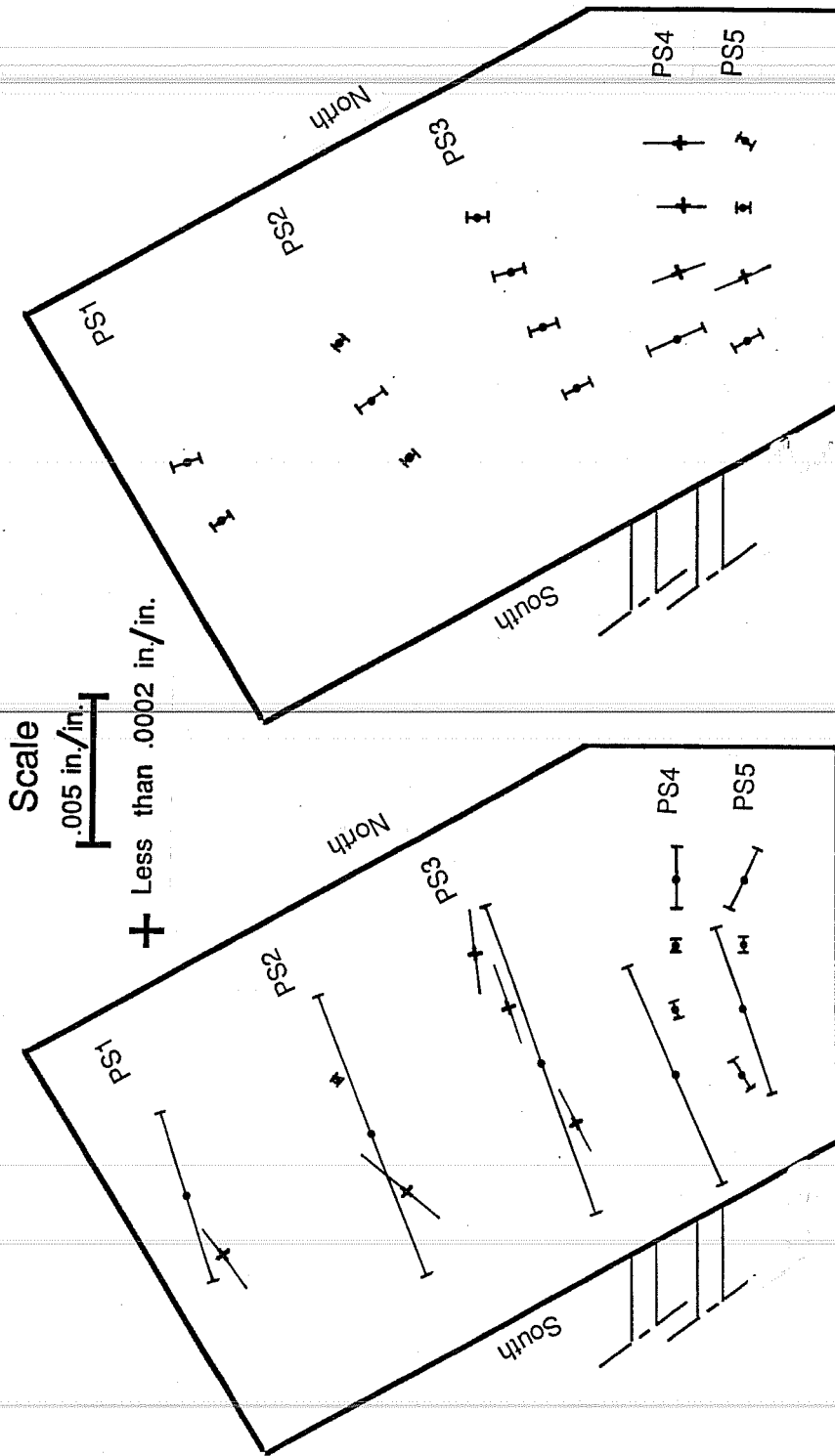


Fig. 4.41 Specimen D2 Principal Surface Strain

	Specimen	Failure Load (kips)	Failure Mode	comments
Series I	A1	260	Compressive	Large Shear Crack at Failure
	B1	260	Anchorage	
	A2	240	Compressive	
	B2	240	Compressive	
	A1-R	350	Compressive	
	A1-2	540	Anchorage	Sudden Failure
Series II	C1	450	Anchorage	Sudden Failure
	C2	415	Anchorage	Sudden Failure
	D1	470	Anchorage	Sudden Failure
	D2	435	Anchorage	Sudden Failure

Table 4.1 Failure Mode of Test Specimens

4.3.1 Failure Mode. With the exception of specimen B2, all the specimens of Series I failed in compression. All Series II specimens experienced a sudden anchorage failure.

4.3.2 Bar force. The load distribution in the bar layers was not uniform. With the exception of the lowest layer of bars of specimen A1-2, none of the reinforcing bars yielded prior to failure.

4.3.3 Surface Strain. The following observations can be made from the surface strain readings:

- 1) Tensile strain coincide with crack locations.
- 2) The compressive strains usually converged to the center at the bottom (reaction) surface.

CHAPTER 5

EVALUATION OF TEST RESULTS

5.1 Introduction

The purpose of this chapter is to evaluate the test results with regard to the observed behavior and mode of failure. The discussion is focused on specimens exhibiting compressive failure, and those exhibiting anchorage failure.

5.2 Node Geometry

The function of the CCT node is to provide for a transfer of forces between the tie, the strut and the support reaction. To perform satisfactorily, the compressive stresses of the strut and those provided by the reaction force must remain below a safe level and the tie must be properly anchored. In designing or checking the node for these two parameters, the geometry of the node must be determined. No experimentally verified guidelines are available to estimate the effective bearing area at a node. Schlaich (18) proposed node geometry based on the strut angle and reinforcement configuration (Fig.5.1a). The drawback of the Schlaich approach is that the center of the effective bearing width (line of action of the load) does not correspond to the center of the real support width. Such a condition will not always be satisfied in practice.

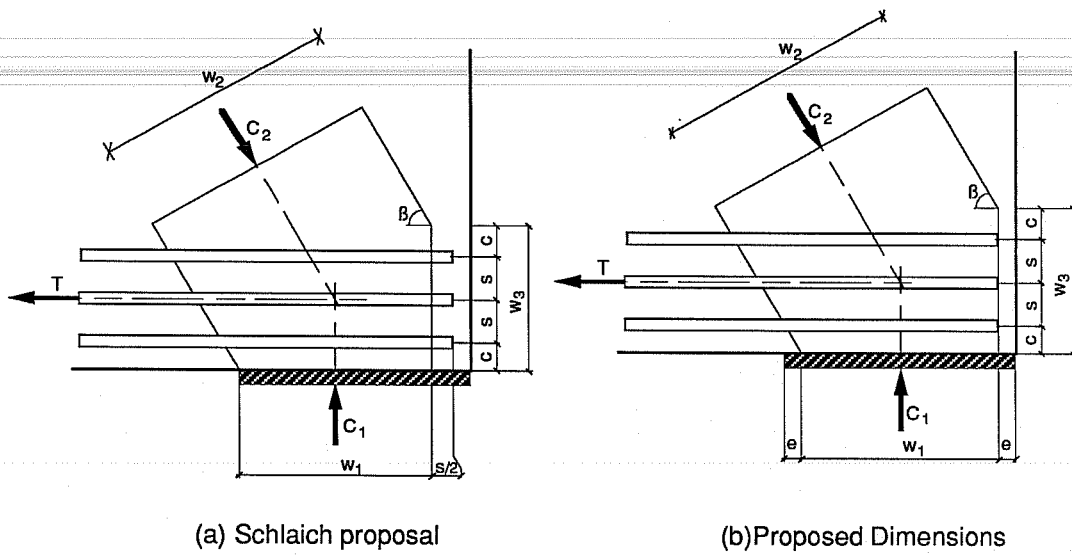


Fig. 5.1 Node Effective Dimensions

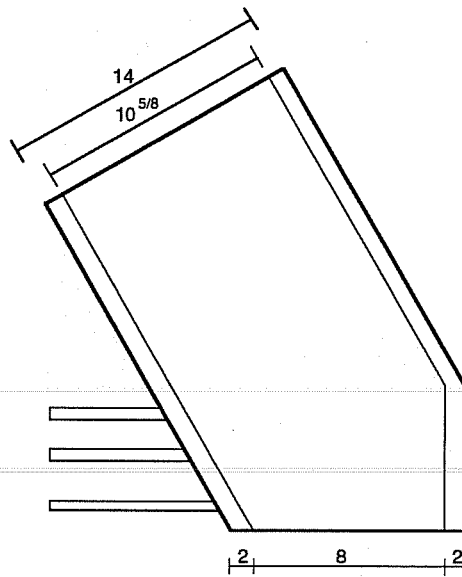


Fig. 5.2 Specimen A1 Effective dimensions

The use of roller is a prime example of such a case. The geometry defined in Figure 5.1b avoids the problem and gives approximately the same results. Based on the geometry shown in Fig.5.1b, effective dimensions of the specimen are given in Table 5.1.

5.3 Specimens Failing in Compression

5.3.1 Experimental Data. Four specimens (A1,A2,B2,A1-R) failed in compression. The strut load on the node was measured experimentally, and the reaction force was calculated from static equilibrium of forces at the node using the geometry defined in Figure 5.1b. The stresses and experimental compressive efficiency factors are summarized in Table 5.3 and were computed using the effective compressive width of the strut and reaction zone.

Although specimen A1 had the same geometry and reinforcement layout as A1-R, it failed at a lower load level because of the thickness of the loading plate (1 in. instead of 2 in.) that caused a stress concentration in the center of the plate and reduced the effective strut width. At failure, the cracks divided the specimen into three segments with the middle segment representing the effective strut (Fig 5.2)

5.3.2 Comparison to existing solutions.

5.3.2.1 Thürlimann (19). Based on tests of beam webs, Thürlimann proposed the following equation for the strut compressive

Specimen	W ₁ (in)	W ₂ (in)	W ₃ (in)
A1	8	10.65	7.44
B1	10	12.38	7.44
A2	6	8.92	7.44
B2	6	8.92	7.44
A1-R	10	12.38	7.44
A1-2	10	12.38	7.44
C1	10	11.19	5.06
C2	10	11.19	5.06
D1	10	12.19	7.06
D2	10	12.19	7.06

Table 5.1 Specimen Dimensions

Specimens	Bar Layer	Anchorage Length	Hook
A1,B1,A1-R	A	10.72	No
	B	12.20	No
	C	13.46	No
A2,B2	A	6.72	No
	B	8.20	No
	C	9.46	No
C1	A	10.72	No
	B	12.20	No
C2	A	10.72	No
	B	12.20	Yes
D1	B	12.20	No
	C	13.46	No
D2	B	12.20	Yes
	C	13.46	No

Table 5.2 Bar development Length

Specimen	f_{28} (psi)	Loading Surface (Measured)		Reaction Surface (Computed)		Efficiency Factor f/f_{28}
		f (psi)	f/f_{28}	f (psi)	f/f_{28}	
A1	2360	2034	0.86	2344	1.00	1.00
A2	2360	2242	0.95	2889	1.22	1.22
B2	2360	2242	0.95	2889	1.22	1.22
A1-R	2360	2322	0.98	2492	1.06	1.06

Table 5.3 Compressive Stresses and Efficiency Factors

Specimen	Compressive Strut Efficiency Factor				
	Experimental	Thürlimann	Mitchell and Collins	Nielsen	Schlaich et. al.
A1	1.00	.65	.72	.72	.80
A2	1.22	.65	.72	.72	.80
B2	1.22	.65	.72	.72	.80
A1-R	1.06	.65	.72	.72	.80

Table 5.4 Experimental and Analytical Efficiency Factors

strength:

$$f_c = .36 f'_c + 700 \text{ psi} \quad \text{for } f'_c \leq 4800 \text{ psi} \quad (5.1)$$

5.3.2.2 Collins and Mitchell (7). Collins and Mitchell based their estimation of the efficiency factor ν for a compression strut on an experimental study made on shear panels. They related the efficiency factor to the principal tensile strength. The equation is as follow :

$$f_c = \nu f'_c \quad (5.2a)$$

$$\nu = \frac{1}{0.8 + 170e_1} \quad (5.2b)$$

$$e_1 = e_x + \frac{e_x + 0.002}{\tan^2 \beta} \quad (5.2c)$$

The principal compressive strain is assumed equal to 0.002

The bar strain (e_x) is conservatively taken as the yield strain.

5.3.2.3 Nielsen et. al (14). Based on an experimental study of web concrete strength Nielsen et al. proposed the following design equation for the efficiency factor:

$$\nu = 0.7 - \frac{f'_c \text{ [psi]}}{29000} \quad (5.3)$$

5.3.2.4 Schlaich et al. (17) Schlaich et al.

proposed an efficiency factor based on the state of strain. Their proposal is incorporated into the proposed draft of the 1990 Comité Euro-International du Béton (CEB) Model Code (MC). In the case of a CCT node, the efficiency factor is:

$$\nu = 0.8 \quad (5.4)$$

5.3.3 Conclusions.

a) Efficiency factor:

All specimen with a compressive failure had an efficiency factor of at least one. This was higher than the factors proposed by different researchers (Table 5.4). Such difference can be due to the fact that the efficiency factors were based on other conditions (thin web, shear panel) and may not be suitable for a CCT node at a beam support.

b) Effect of transverse reinforcement:

Specimen B1 was similar to specimen A1-R (and to A1) but did not have any transverse reinforcement. It failed in anchorage at a lower load than A1-R. The role of transverse reinforcement is critical in increasing the bond anchorage capacity of the tie and developing a compressive failure at the node.

c) Effect of the size of the reaction area:

The tests suggest that a decrease in the loading (and

reaction) area increases the efficiency factor. The use of a smaller bearing area increased the compressive strength of the strut in specimens A2 (compared to specimens A1-R and A1) and B2 (compared to specimen A2) by about 20%

5.4 Specimen Failing in Anchorage

5.4.1 Experimental Data. Six specimens, including all series II specimens, (B1, A1-2, C1, C2, D1, D2) experienced anchorage failures. All of the specimens failed before bar yielding with the exception of specimen A1-2.

5.4.2 Effective Anchorage Lengths. The effective anchorage length is measured from the boundary of the effective node. The effective length is summarized in Table 5.2.

5.4.3 Required Anchorage Length (ACI 318-83). The effective length were checked against ACI 318 requirements. The current ACI code expressions for development length for 60 ksi bars are as follow:

a) straight bars:

$$l_{db} = 0.04 \frac{A_b f_y}{\sqrt{f'_c}} \quad (5.5)$$

b) hooked bars :

$$l_{db} = 1200 \frac{d_b}{\sqrt{f'_c}} \quad (5.6)$$

Using nominal value for f_y (60 ksi), ACI 318-83 required bar lengths are summarized in Table 5.5.

5.4.4 Required Anchorage Length Using ACI 408. ACI committee 408 proposed a development length based on a statistical analysis of experimental data presented by Orangun et. al. (15). The proposed formula considered the important parameters that influence the development length. The following expression was used for straight bars :

$$\frac{u}{\sqrt{f'_c}} = 1.2 + \frac{3C}{d_b} + \frac{50d_b}{l} + \frac{A_{tr} f_{yt}}{500s d_b} \quad (5.7)$$

and

$$u = \frac{d_b f_y}{4l_d} \quad (5.8)$$

where :

C : cover parameter.

d_b : bar diameter

l : bar length

A_{tr} : area of transverse reinforcement crossing plane of splitting.

s : maximum spacing of transverse reinforcement within l_d , center to center

Table 5.5 shows the computed values.

5.4.5 Comparison.

Specimen	Bar Layer	Provided L_p	ACI 318 L_3	L_p/L_3	ACI 408 L_4	L_p/L_4
B1	A	10.72	15	.71	23	.46
	B	12.20	22	.55	37.5	.33
	C	13.46	22	.61	37.5	.36
A1-2	A	10.72	11	.97	15	.71
	B	12.20	15	.81	24	.51
	C	13.46	15	.90	24	.56
C1	A	10.72	21	.51	31	.35
	B	12.20	21	.58	23	.53
C2	A	10.72	15	.71	10	> 1
	B	12.20	21	.58	31	.39
D1	B	12.20	21	.58	31	.39
	C	13.46	21	.64	23	.59
D2	B	12.20	15	.81	10	> 1
	C	13.46	21	.64	31	.43

Table 5.5 Specimens with Anchorage Failure : Provided and Computed Anchorage Length to Provide Yield
($f_y = 60$ ksi)

Specimen	Failure Load / Yield Load		
	Measured	ACI 318	ACI 408
B1	.43	.55	.33
A1-2	.92	.81	.51
C1	.77	.51	.35
C2	.80	.58	.39
D1	1.04	.58	.39
D2	1.01	.64	.43

Table 5.6 Specimen with Anchorage Failure Computed and Measured Force in Bars at Failure
($f_y = 60$ ksi)

Table 5.6 summarizes the computed (ACI 318 and ACI 408) and measured failure load versus yield load ratio. Table 5.7 gives the measured versus computed failure load ratio.

To illustrate the procedure used in developing the values of Tables 5.6 and 5.7, detailed computations for specimen B1 will be shown. The anchorage lengths (denoted L_p) of the layer A,B, and C of specimen B1 are 10.72, 10.22 and 13.46 in., respectively. The lengths (L_3) required by ACI 318 to develop yield ($f_y=60$ ksi) are 15, 22, and 22 in. The ratios of provided length (L_p) to required length (L_3) to develop yield are then computed and are .71, .55, and .61 for layer A,B, and C respectively. Assuming that the bond strength is constant along the bar length, the bars of layer B will trigger an anchorage failure when the level of the stresses on the bars reach $.55f_y$. This value is then reported in Table 5.6. The same type of computations is followed using ACI 408 recommendations.

The yield failure of specimen B1 was computed assuming a uniform distribution of stresses on the bars. Since the specimen was reinforced with 8#6 and 3#5 bars, the bar force needed to develop yield is:

$$F_y = [8(.44) + 3(.31)] * 60 = 267 \text{ kips}$$

The measured total bar force (F) is expressed as a

Specimen	Measured P_m (kips)	ACI 318 P_3 (kips)	P_3/P_m	ACI 408 P_4 (kips)	P_4/P_m
B1	145	147	1.01	88	.61
A1-2	245	216	.87	136	.56
C1	167	110	.65	76	.46
C2	174	110	.63	76	.44
D1	204	125	.61	84	.41
D2	213	125	.59	84	.39

Table 5.7 Comparison Between Computed and Measured Force in Bars

Specimen	$\frac{u}{\sqrt{f'_c}}$	$\sqrt{f_n}$	β
B1	8.93	32.91	.31
A1-2	13.23	47.43	.02
C1	17.60	43.30	.17
D1	15.43	44.25	.13

Table 5.8 Effect of Lateral Pressure

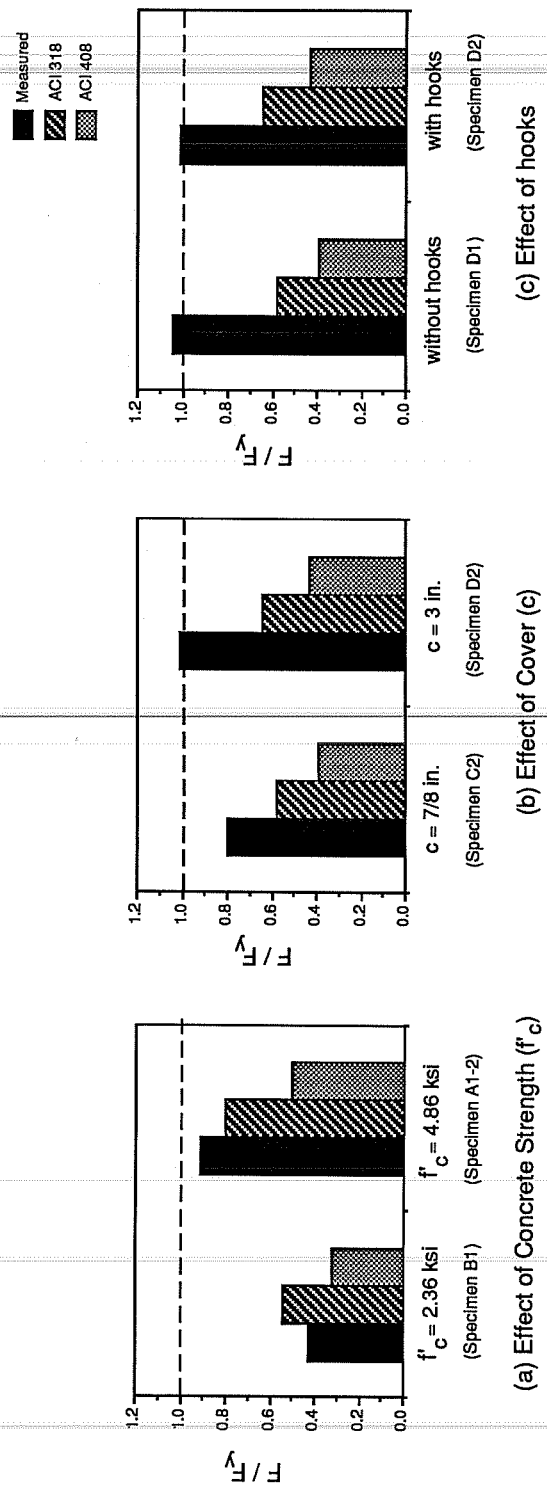


Fig. 5.3 Specimens with Anchorage Failure: Ratio of Total Bar Force at Failure (F) to Yield Force (F_y)

fraction of F_y and is reported in Table 5.6. That value was .43 for specimen B1.

To better emphasize the effect of the different parameters involved (concrete strength, cover, and use of hooks), bar graphs were drawn (Fig.5.3). Those graphs indicates the following:

1) An increase in the concrete strength from 2.36 ksi to 4.86 ksi, increased the specimen capacity by 46%

2) An increase in the cover (from 7/8 in. to 3 in.), which implied also an increase in the bar development length, improved the specimen capacity by an average of 24%

3) The use of 180° standard ACI hook had no effect on the specimen capacity.

The graph (Fig.5.3) shows how the measured values compare to the values computed using either the ACI 318 requirements or the ACI 408 recommendations.

5.4.5.1 Comparison to ACI 318 Requirements. The values using ACI 318 are conservative except for the specimen A1-2 which was in good agreement.

5.4.5.2 Comparison to ACI 408 Recommendations. The ACI 408 recommendations gave very conservative results. The lateral pressure from the reaction was the most likely factor that increased the anchorage strength of the tie. To explore the effect of the

lateral pressure, Equation 5.7 was modified as follows:

$$\frac{u_1}{\sqrt{f'_c}} = \frac{u}{\sqrt{f'_c}} + \beta\sqrt{f_n} \quad (5.9)$$

f_n is the lateral pressure

u is the bond strength using ACI 408.

In order to obtain a satisfactory anchorage the bond strength should be:

$$u_1 = \frac{d_b f_y}{4l_d} \quad (5.10)$$

The factor (β) is then

$$\beta = \frac{u_1 - u}{\sqrt{f_n f'_c}} \quad (5.11)$$

The value of (β) summarized in Table 5.8 do not show any definite trend but may help explain the anchorage values of the tests.

5.4.6 Conclusions. Specimens D1 and D2 failed at a higher load than specimens C1 and C2, respectively, since they had longer development length.

The specimens with hooked bars (D1 and D2) failed at a lower load than the those with straight bars (C1 and C2). However,

this does not imply that the use of straight bars increases the capacity. It is likely that in this study the boundary conditions were changed when the node was isolated for testing purpose and this had a negative effect on the bond resistance.

5.5 Need for Further Research.

The compressive strut efficiency factor obtained by this experimental study may not be suitable for high strength concrete since the concrete strength used for the specimens that failed in compression was less than 3 ksi. Additional research needs to be conducted in order to estimate the effect of concrete compressive strength on the efficiency factor.

In order to evaluate the effect of concrete crushing and anchorage failure on the CCT node, none of the specimens was loaded to yielding of the longitudinal bars. Additional experimental work needs to be implemented in order to evaluate the effect of bar yielding on the behavior of the CCT node specially since in design yielding of the bars should be reached before crushing of the concrete occurs.

CHAPTER 6

CONCLUSIONS

6.1 Introduction

The purpose of this investigation was to examine the behavior of the compressive-Compressive-Tensile (CCT) nodes of the strut and tie model. The CCT node was isolated from the end reaction region of a prototype dapped beam. This study was aimed at defining the geometry of the node, the effect of the level of compressive stresses, and the influence of the anchorage of the tensile tie.

Ten specimens were tested. The parameters that were investigated are the concrete strength, the size of bearing area, the use of transverse reinforcement, the longitudinal reinforcement configuration, and the use of hooks for the longitudinal bars.

The experimental results were checked against available analytical models.

6.2 Conclusions and Recommendations

1) Failure modes: Two failure modes were observed for the CCT node specimens: anchorage failure and compressive failure. Anchorage failure was due to inadequate bar development length. The appearance of the specimen at failure and the crack pattern clearly indicated which mode controlled in each case.

2) Specimen geometry: The primary element in designing a CCT node is the determination of its geometry. The strut angle was chosen according to the design model for the dapped beam. Tests of dapped beams designed using the strut and tie model approach indicated that the strut developed in the beam was oriented as assumed in the design calculations. The effective bearing area was based on a theoretical model proposed by Schlaich (2). This model gave consistent results for evaluating the tie anchorage characteristics and the effective compressive strength factor of the strut.

3) Compressive strength efficiency factor: The measured efficiency factor (the ratio of average compressive stresses on the strut to the concrete strength) for compression failure was found to be at least equal to 1.0 and to increase with a reduction in the size of the bearing area. The specimens with a large bearing area had an efficiency factor of 1.0 and specimens with a reduced bearing area had an efficiency factor of 1.20. Available models were conservative in the determination of the efficiency factor for the specimens in this study. A factor of 1.0 is proposed for design of CCT nodes of the type tested herein.

4) Transverse reinforcement: The experimental study showed that the transverse reinforcement restrained the cracks and

increased the capacity by 35% by preventing an anchorage failure.

5) Anchorage: The anchorage lengths proposed by ACI 318 (1) and ACI 408 (11) were found to be very conservative. The use of hooks did not increase the capacity of the specimens in this study, however the cover and the spacing also were varied and may have changed the anchorage conditions of the hooked bars relative to the straight bars.

BIBLIOGRAPHY

1. American Concrete Institute, *Building Code Requirements for Reinforced Concrete* (ACI 318-83), Detroit, 1983
2. Anderson, R.B., *Behavior of CCT-Nodes in Reinforced Concrete Strut-And-Tie Models* Master Thesis, The University of Texas at Austin, December 1988.
3. Barton, D.L., *Detailing of Structural Concrete Dapped End Beams*, Master Thesis, The University of Texas at Austin, December 1988.
4. Bergmeister, K., Breen, J.E., Jirsa, J.O., Kreger, M.E., "Detailing for Structural Concrete", unpublished *Research Report 1127-3F* Center for Transportation Research, The University of Texas at Austin,
5. *C.E.B.-F.I.P. Model Code 1990 First Predraft 1988*, Comité Euro-International du Béton, *Bulletin d'Information* No 190b, July 1988.
6. Collins, M.P., and Mitchell, D. "Towards a Rational Theory for Reinforced Concrete Members in Shear", *ASCE Proceedings*, Vol. 104, St. 4, April 1978, pp. 649-666.
7. Collins, M.P., and Mitchell D., "A Rational Approach to Shear Design- The 1984 Canadian Provisions", *ACI Journal*, Vol 83 No 6, Nov-Dec 1986, pp.925-933.
8. Cook, W.D., and Mitchell, D. "Studies of Disturbed Regions near Discontinuities in Reinforced Concrete Members", *ACI Structural Journal*, Vol 88 No 2, March-April 1988, pp.206-216.
9. Jirsa, J.O., Lutz, L.A., Gargely, P., "Rationale for suggested Development, Splice, and Standards Hook Provisions for Deformed Bars in Tension", *Concrete International*, Vol 1, No 7, July 1979, pp.47-61.
10. Lormanometee, S., *Bond Strength of Deformed Reinforcing Bar Under Lateral Pressure*, Master Thesis, The University of

Texas at Austin, Jan. 1974.

11. Marti, P., "Basic Tools of Reinforced Concrete Design", *ACI Journal*, Vol 82 No 1, Jan-Feb 1985, pp.46-56.
12. Marti, P., "Truss Model in Detailing", *Concrete International*, Vol 7 No 12, Dec. 1985, pp.66-73.
13. Mörsch, E. *Der Eisenbetonbau-Seine Theorie und Anwendung*, (Reinforced Concrete Theory), Verlag Konrad Wittwer, Stuttgart, 1912.
14. Nielson, M., Braestrup, N., Jensen, B., and Bach, F., *Concrete Plasticity: Beam Shear-Shear in Joints-Punching Shear*, Specialpublikation Dansk Selskab for Bygningsstatik, Lyngby, 1978.
15. Orangun, C.O., and Jirsa, J.O., and Breen, J.E., "A Reevaluation of Test Data on Development Length and Splices", *ACI Journal*, vol. 74 No 3 March 1977, pp.114-122
16. Ritter, W., "Die Bauweise Hennebique"(The Hennebique Design Method), *Schweizerische Bauzeitung*, Zürich, Vol. 33 No 7, Feb. 1899.
17. Schlaich, J., Schafer, K., Jennewein, M. "Toward a Consistent Design of Structural Concrete", *PCI Journal*, Vol 32 No 3, May-June 1987 pp.75-149.
18. Schlaich, J. and Schäfer, K., "Konstruieren im Stahlbetonbau" (Concrete Structure Design) *Betonkalender*, Berlin, 1989, pp. 563-715.
19. Thürlimann, B., *Lectures Notes for Structural Seminar*, The University of Texas at Austin
20. Thürlimann, B., Marti, P., Pralong, J., Ritz, P., Zimmerli, B., *Anwendung der Plastizitätstheorie auf Stahlbeton* (Plasticity in Concrete Structures), Volesung, ETH-Zürich, 1983
21. Vecchio, F.J. and Collins, M.P., "The modified Compression Field Theory for Reinforced Concrete Elements Subjected to Shear", *ACI Journal*, Vol 83 No 2, March-April 1986, pp. 219-231.

22. Vechio, F.J. and Collins, M.P., "Predicting the response of Reinforced Concrete Beams Subjected to Shear Using Modified Compression Field Theory", *ACI structural Journal*, May-June 1988, pp.258-268.

VITA

Abdelhakim Bouadi was born on November 4, 1961 in Algiers, Algeria, the son of Mohand Bouadi and Taos Messara. After completing his high school, he entered the *Ecole Polytechnique d'Alger*. He received his *Ingeniorat* (Bachelor) of Civil Engineering from the *Ecole Polytechnique* in June 1985. He entered the Graduate School of the University of Texas at Austin in September 1986.

Permanent Address: 68 Rue Jean Jaures
El Mouradia, 16070
Algiers, Algeria